Supporting Information

Bridging D–A type photosensitizers with the azo group to boost intersystem crossing for efficient photodynamic therapy

Boyi Hao,[1] Jiaxin Wang,[1] Chao Wang,[1] Ke Xue,[1] Minghui Xiao,[1] Shuyi Lv,[1] and Chunlei Zhu[1,*]

[1]Key Laboratory of Functional Polymer Materials of Ministry of Education, State Key Laboratory of Medicinal Chemical Biology, Institute of Polymer Chemistry, College of Chemistry, Nankai University, Tianjin 300071, China

Email: chunlei.zhu@nankai.edu.cn

Experimental Section

Chemicals and materials. Aniline, *tetrakis*(triphenylphosphine)palladium ($Pd(PPh_3)_4$), *bis*(triphenylphosphine)palladium(II) chloride ($PdCl_2(PPh_3)_2$), pyridine-4-boronic acid, and potassium peroxymonosulfate were obtained from Energy Chemical. Phenanthroline, cuprous chloride, potassium acetate, 4-(5-bromothiophen-2-yl)pyridine, *bis*(pinacolatodiborane), 2,5-dibromothiophen, and 4-pyridylboronic acid were ordered from Heowns. 4-Aminophenylboronic acid pinacol ester, 1-bromo-4-iodobenze, 5,5-dimethyl-1-pyrroline N-oxide (DMPO) and were purchased from Biodepharm. 2',7'-Dichlorofluorescin diacetate (DCFH-DA) and 9,10-anthracenediyl-*bis*(methylene)-dimalonic acid (ABDA) were purchased from Sigma-Aldrich. Dihydrorhodamine 123 (DHR-123) and vitamin C (Vc) were ordered from Maclin and Solarbio, respectively. Iodomethane (CH_3I), dry tetrahydrofuran (THF), and dimethyl sulfoxide (DMSO) were ordered from Adamas. Dichloromethane (DCM), methoxymethane (DME), ethyl acetate, petroleum ether, toluene, acetonitrile, acetone, potassium hydroxide (KOH), potassium carbonate (K_2CO_3), magnesium sulfate ($MgSO_4$), chloride solution (NaCl), and sodium sulfate (Na_2SO_4) were purchased from Tianjin Bohai Chemical Industry Group. All chemicals were used as received without further purification. The water used in all experiments was obtained by filtering through a set of HEAL FORCE cartridges (Smart-N15VF).

Synthesis of TPA-Th(+). Compound **1** was prepared according to a previously reported procedure.[1] Briefly, aniline (466 mg, 5 mmol), 1-bromo-4-iodobenze (2.1 g, 7.5 mmol), phenanthroline (90 mg, 0.5 mmol), cuprous chloride (50 mg, 0.5 mmol), and KOH (2.2 g, 40 mmol) were mixed under nitrogen atmosphere, followed by the addition of degassed toluene (10 mL) using a syringe. The mixture was heated to 120 °C and then stirred at reflux for 12 h. After cooling to ambient temperature, the mixture was washed with water, dried over anhydrous $MgSO_4$, and concentrated under reduced pressure. The crude product was purified on a silica-gel column (petroleum ether) to afford compound **1** in 23% yield.

Compound **2** was synthesized by referring to a previously published paper.[2] Briefly, 2,5-

dibromothiophen (4.8 g, 20 mmol), 4-pyridylboronic acid (1.2 g, 10 mmol), $Pd(PPh_3)_4$ (578 mg, 0.5 mmol), and K_2CO_3 (11.1 g, 80 mmol) were added to the mixture of DME (45 mL) and water (15 mL). The reaction system was refluxed at 90 °C for 12 h under nitrogen atmosphere, followed by concentrating under reduced pressure. The crude product was purified on a silica-gel column (petroleum ether) to afford a white solid (*i.e.*, 4-(5-bromo-2-thienyl)pyridine). Next, *bis*(pinacolatodiborane) (7.6 g, 30 mmol), 4-(5-bromo-2-thienyl)pyridine (2.4 g, 10 mmol), potassium acetate (7.8 g, 80 mmol), and $PdCl_2(PPh_3)_2$ (673 mg, 0.96 mmol) were added to dry dioxane (60 mL). After degassing, the reaction system was stirred at 85 °C overnight under nitrogen atmosphere. Next, the crude product was filtrated through celite, concentrated under reduced pressure, and purified on a silica-gel column (DCM) to afford an orange solid (compound **2**) in 76% yield.

Compound **1** (4.2 g, 10.5 mmol) and compound **2** (2.0 g, 7 mmol) were dissolved in the degassed mixture of THF (15 mL) and water (5 mL). After the addition of $Pd(PPh_3)_4$ (405 mg, 0.35 mmol) and K_2CO_3 (3.8 g, 28 mmol), the reaction system was stirred at ambient temperature for 5 min. Next, the mixture was heated to 70 °C and stirred at reflux overnight. After cooling to ambient temperature, the mixture was extracted with chloroform and washed with saturated NaCl solution. The organic layer was then dried over anhydrous Na_2SO_4 and concentrated under reduced pressure. The crude product was purified on a silica-gel column (DCM/methanol = 80/1) to afford a light-yellow solid (compound **3**) in 48% yield. ^{1}H-NMR (400 MHz, $CDCl_3$): δ 8.58 (d, 2H), 7.52–7.45 (m, 5H), 7.36 (d, 2H), 7.31–7.23 (m, 3H), 7.09 (dd, 8.2 Hz, 5H), 6.99 (d, 2H). ^{13}C-NMR (100 MHz, $CDCl_3$): δ 150.41, 147.45, 146.92, 146.53, 146.02, 141.33, 139.30, 132.40, 129.60, 128.10, 126.81, 126.45, 125.77, 124.94, 123.92, 123.68, 123.56, 119.44, 115.65. HRMS (ESI, m/z, $C_{27}H_{19}BrN_2S$, $[M - Br]^+$): calcd., 482.0452; found, 483.0527.

Compound **3** (500 mg, 1 mmol) and 4-aminophenylboronic acid pinacol ester (329 mg, 1.5 mmol) were dissolved in the degassed mixture of THF (15 mL) and water (3 mL), followed by the addition of $Pd(PPh_3)_4$ (58 mg, 0.05 mmol) and K_2CO_3 (830 mg, 6 mmol). Next, the reaction system was stirred at 70 °C for 8 h. After cooling to ambient temperature, the reaction mixture was

extracted with chloroform and washed with water. The organic layer was dried over anhydrous Na_2SO_4 and concentrated under reduced pressure. The crude product was purified on a silica-gel column (DCM/methanol = 50/1) to afford an orange solid (compound **4**) in 60% yield. ^{1}H-NMR (400 MHz, $CDCl_3$): δ 8.76–8.63 (m, 2H), 7.83–7.75 (m, 2H), 7.64 (d, 1H), 7.57 (t, 8H), 7.50 (d, 2H), 7.39 (t, *J* = 7.7 Hz, 2H), 7.33 (d, 1H), 7.28 (s, 1H), 7.25–7.15 (m, 4H), 6.84 (d, 2H). ^{13}C-NMR (100 MHz, $CDCl_3$): δ 150.27, 147.99, 147.31, 146.43, 145.75, 145.60, 138.93, 136.35, 132.20, 132.11, 131.97, 130.86, 128.62, 128.50, 127.65, 127.21, 126.70, 126.55, 125.08, 124.77, 123.43, 123.20, 115.48. HRMS (ESI, m/z, $C_{33}H_{25}N_3S$, $[M + H]^+$): calcd., 495.1769; found, 496.1819.

Compound **4** (250 mg, 0.5 mmol) was dissolved in acetonitrile (20 mL), followed by the addition of CH_3I (300 mg). Next, the reaction system was stirred at 70 °C for 4 h. After cooling to ambient temperature, the reaction mixture was concentrated under reduced pressure. The crude product was purified on a silica-gel column (DCM/methanol = 10/1) to afford a red solid (denoted as TPA-Th(+)) in 73% yield. ^{1}H-NMR (400 MHz, $CDCl_3$): δ 8.70–8.63 (m, 2H), 8.15 (dd, 2H), 8.08 (dd, 1H), 7.68–7.60 (m, 2H), 7.56–7.47 (m, 4H), 7.43 (d, 1H), 7.34 (t, 2H), 7.19–7.03 (m, 7H), 6.86 (d, 1H), 6.73 (d, 1H), 4.29 (s, 3H). ^{13}C-NMR (100 MHz, $CDCl_3$): δ 153.08, 148.42, 147.91, 146.73, 146.49, 144.37, 139.02, 135.18, 134.42, 133.80, 132.13, 129.42, 127.51, 126.64, 125.65, 125.02, 124.75, 124.03, 123.62, 122.89, 121.17, 120.38, 115.42, 46.24. HRMS (ESI, m/z, $C_{34}H_{28}N_3S^+$, [M]): calcd., 510.1998; found, 510.2049.

Synthesis of Azo-TPA-Th(+). Compound **5** was prepared according to a previously reported procedure.[3] Briefly, 4-bromoaniline (3.5 g, 20 mmol) was dissolved in DCM, followed by the addition of aqueous potassium peroxymonosulfate solution (12.25 wt.%, 200 mL). The reaction system was stirred at 37 °C for 5 h. Next, the reaction was filtrated through celite and the residue was washed with DCM and dried over anhydrous Na_2SO_4. After concentrating under reduced pressure, the crude product was purified on a silica-gel column (petroleum ether) to give 4,4'-dibromo-azobenzene. 4,4'-Dibromo-azobenzene (1 g, 4 mmol), *bis*(pinacolatodiborane) (3 g, 12 mmol), potassium acetate (3.1 g, 32 mmol), and $PdCl_2(PPh_3)_2$ (28 mg, 0.04 mmol) were mixed

with dry dioxane (20 mL). After degassing, the reaction system was stirred at 85 °C overnight under nitrogen atmosphere. Next, the crude product was filtrated through celite, concentrated under reduced pressure, and purified on a silica-gel column (DCM) to afford an orange solid (compound **5**) in 64% yield.

Compound **5** (434 mg 1 mmol) and compound **3** (750 mg, 1.5 mmol) were dissolved in the degassed mixture of THF (15 mL) and water (5 mL), followed by the addition of $Pd(PPh_3)_4$ (58 mg, 0.05 mmol) and K_2CO_3 (415 mg, 3 mmol). Next, the reaction system was stirred at 70 °C for 8 h. After cooling to ambient temperature, the reaction mixture was extracted with chloroform and washed with saturated NaCl solution. The organic layer was dried over anhydrous Na_2SO_4 and concentrated under reduced pressure. The crude product was purified on a silica-gel column (DCM/methanol = 20/1) to afford a red solid (compound **6**) in 16% yield. ^{1}H-NMR (400 MHz, $CDCl_3$): δ 8.63 (d, 2H), 8.04–7.99 (m, 1H), 7.75 (d, 2H), 7.60 (d, 2H), 7.52 (qd, 6H), 7.36–7.29 (m, 2H), 7.23–7.09 (m, 8H). ^{13}C-NMR (100 MHz, $CDCl_3$): δ 151.73, 149.03, 148.82, 147.09, 146.88, 142.89, 134.92, 130.82, 129.69, 129.66, 128.12, 127.97, 127.94, 127.27, 125.52, 124.80, 124.67, 124.30, 123.58, 123.55, 123.33, 121.20, 116.26. HRMS (ESI, m/z, $C_{66}H_{46}N_6S_2$, $[M + H]^+$): calcd., 986.3225; found, 987.3296.

Compound **6** (50 mg, 0.05 mmol) was dissolved in acetonitrile (10 mL), followed by the addition of CH_3I (30 mg). Next, the reaction system was stirred at 70 °C for 4 h. After cooling to ambient temperature, the reaction mixture was concentrated under reduced pressure. The crude product was purified on an alumina column (DCM/methanol = 40/1) to afford a red solid (denoted as Azo-TPA-Th(+)) in 64% yield. ^{1}H-NMR (400 MHz, DMSO-d_6): δ 8.86 (d, J = 6.4 Hz, 2H), 8.19 (d, J = 6.5 Hz, 3H), 7.87–7.78 (m, 2H), 7.66 (d, J = 8.6 Hz, 2H), 7.51 (td, 3H), 7.38 (t, J = 7.8 Hz, 2H), 7.19–7.08 (m, 4H), 7.01 (dd, J = 10.7, 8.4 Hz, 5H), 4.25 (s, 3H). ^{13}C-NMR (100 MHz, DMSO-d_6): δ 151.40, 148.47, 147.75, 146.66, 146.11, 145.81, 145.52, 142.66, 134.10, 134.28, 130.44, 128.57, 128.16, 127.73, 127.60, 126.66, 126.09, 125.91, 125.07, 124.75, 123.79, 123.29, 121.80, 47.17. HRMS (ESI, m/z, $C_{68}H_{52}N_6S_2^{2+}$, $[M]^{2+}$): calcd., 508.1842; found, 508.1846.

Synthesis of TPA(+). Compound **1** (1.2 g, 3 mmol), pyridine-4-boronic acid (246 mg, 2 mmol), $Pd(PPh_3)_4$ (173 mg, 0.15 mmol), and K_2CO_3 (830 mg, 6 mmol) were added to the mixture of DME (15 mL) and water (5 mL). The reaction system was refluxed at 90 °C for 12 h under nitrogen atmosphere, followed by concentrating under reduced pressure. The crude product was purified on a silica-gel column (DCM/methanol = 100/1) to afford compound **7** in 76% yield. ^{1}H-NMR (400 MHz, $CDCl_3$): δ 8.62 (d, *J* = 6.0 Hz, 2H), 7.54 (d, *J* = 8.7 Hz, 2H), 7.51–7.45 (m, 5H), 7.41 (d, *J* = 8.5 Hz, 2H), 7.31 (t, *J* = 7.9 Hz, 2H), 7.23–7.15 (m, 7H), 7.09 (d, *J* = 14.6 Hz, 1H), 6.76 (d, *J* = 8.5 Hz, 2H). ^{13}C-NMR (100 MHz, $CDCl_3$): δ 150.28, 148.48, 147.52, 146.87, 146.48, 132.48, 131.70, 129.68, 129.51, 127.88, 126.01, 125.16, 124.14, 123.40, 115.93. HRMS (ESI, m/z, $C_{23}H_{19}BrN_2S$, $[M - Br]^+$): calcd., 400.0575; found, 401.0640.

Compound **7** (401 mg, 1 mmol) and 4-aminophenylboronic acid pinacol ester (329 mg, 1.5 mmol) were dissolved in the degassed mixture of THF (15 mL) and water (5 mL), followed by the addition of $Pd(PPh_3)_4$ (58 mg, 0.05 mmol) and K_2CO_3 (830 mg, 6 mmol). Next, the reaction system was stirred at 70 °C for 8 h. After cooling to ambient temperature, the reaction mixture was extracted with chloroform and washed with water. The organic layer was dried over anhydrous Na_2SO_4 and concentrated under reduced pressure. The crude product was purified on a silica-gel column (DCM/methanol = 70/1) to afford a white solid (compound **8**) in 83% yield. ^{1}H-NMR (400 MHz, $CDCl_3$): δ 8.63–8.60 (m, 2H), 7.55–7.51 (m, 2H), 7.50–7.44 (m, 5H), 7.42–7.39 (m, 2H), 7.33–7.27 (m, 3H), 7.20–7.14 (m, 6H), 7.12–7.05 (m, 1H), 6.78–6.73 (m, 2H). ^{13}C-NMR (100 MHz, $CDCl_3$): δ 150.16, 148.99, 147.76, 147.25, 145.70, 145.54, 136.54, 130.90, 130.86, 129.47, 127.67, 127.24, 125.28, 124.99, 123.61, 122.88, 120.90, 115.47. HRMS (ESI, m/z, $C_{29}H_{23}N_3$, $[M + H]^+$): calcd., 413.1892; found, 414.1963.

Compound **8** (207 mg, 0.5 mmol) was dissolved in acetonitrile (10 mL), followed by the addition of CH_3I (300 mg). Next, the reaction system was stirred at 70 °C for 4 h. After cooling to ambient temperature, the reaction mixture was concentrated under reduced pressure. The crude product was purified on a silica-gel column (DCM/methanol = 30/1) to afford a yellow solid (denoted as TPA(+)) in 83% yield. ^{1}H-NMR (400 MHz, CD_3OD): δ 8.65 (dd, 2H), 8.19 (dd, 2H),

7.86 (dd, *J* = 9.0 Hz, 2H), 7.51 (dd, 3H), 7.43–7.34 (m, 3H), 7.24–7.13 (m, 5H), 7.07 (dd, 2H), 6.80 (dd, 1H), 6.67 (d, 1H), 4.28 (s, 3H). ^{13}C-NMR (100 MHz, CD_3OD): δ 154.88, 152.06, 149.98, 146.06, 144.55, 144.02, 138.08, 129.56, 129.00, 127.73, 126.92, 126.26, 126.01, 125.00, 124.28, 122.25, 120.42, 119.95, 113.10, 46.13. HRMS (ESI, m/z, $C_{36}H_{26}N_3^+$, $[M]^+$): calcd., 428.2121; found, 428.2122.

Synthesis of Azo-TPA(+). Compound **7** (401 mg 1 mmol) and compound **5** (651 mg, 1.5 mmol) were dissolved in the degassed mixture of THF (15 mL) and water (3 mL), followed by the addition of $Pd(PPh_3)_4$ (58 mg, 0.05 mmol) and K_2CO_3 (415 mg, 3 mmol). Next, the reaction system was stirred at 70 °C for 8 h. After cooling to ambient temperature, the reaction mixture was extracted with chloroform and washed with saturated NaCl solution. The organic layer was dried over anhydrous Na_2SO_4 and concentrated under reduced pressure. The crude product was purified on a silica-gel column (DCM/methanol = 50/1) to afford an orange solid (compound **9**) in 43% yield. ^{1}H-NMR (400 MHz, $CDCl_3$): δ 8.62 (d, *J* = 5.2 Hz, 2H), 8.02–7.89 (m, 2H), 7.73 (dd, *J* = 8.8, 2.4 Hz, 2H), 7.60–7.53 (m, 4H), 7.49 (d, *J* = 5.1 Hz, 2H), 7.32 (t, *J* = 7.8 Hz, 2H), 7.23–7.18 (m, 6H), 7.12 (t, *J* = 7.4 Hz, 1H). ^{13}C-NMR (100 MHz, $CDCl_3$): δ 151.73, 149.03, 147.09, 146.88, 142.89, 134.92, 130.82, 129.69, 128.12, 128.07, 127.97, 127.94, 127.27, 125.52, 124.67, 124.30, 123.55, 123.33, 123.18, 116.25. HRMS (ESI, m/z, $C_{58}H_{42}N_6$, $[M + H]^+$): calcd., 822.3471; found, 823.3534.

Compound **9** (330 mg, 0.4 mmol) was dissolved in acetonitrile (10 mL), followed by the addition of CH_3I (300 mg). Next, the reaction system was stirred at 70 °C for 4 h. After cooling to ambient temperature, the reaction mixture was concentrated under reduced pressure. The crude product was purified on an alumina column (DCM/methanol = 20/1) to afford a red solid (denoted as Azo-TPA (+)) in 76% yield. ^{1}H-NMR (400 MHz, DMSO-d_6): δ 8.71 (d, *J* = 6.7 Hz, 2H), 8.26 (d, *J* = 6.8 Hz, 2H), 8.01–7.97 (m, 2H), 7.95–7.89 (m, 2H), 7.83–7.80 (m, 2H), 7.75–7.71 (m, 2H), 7.41 (t, *J* = 7.8 Hz, 2H), 7.27–7.20 (m, 5H), 7.18–7.13 (m, 2H), 4.31 (s, 3H). ^{13}C-NMR (100 MHz, DMSO-d_6): δ 153.68, 151.53, 151.18, 146.41, 146.06, 145.64, 142.56, 135.28, 130.62, 130.02, 128.77, 127.80, 126.76, 125.99, 125.74, 123.81, 122.87, 121.27, 47.11. HRMS (ESI, m/z,

$C_{60}H_{48}N_6^{2+}$, $[M]^{2+}$): calcd., 426.1965; found, 426.1971.

Characterizations. The absorption and emission spectra of all samples were measured by a UV/vis spectrometer (UV-2600, Shimadzu) and a fluorometer (F-4700, HITACHI), respectively. The particle size distribution was characterized by dynamic light scattering (DLS; Zetasizer Nano ZS90, Malvern).

Theoretical calculations. Geometry optimization was performed using the density functional theory (DFT) at B3LYP/6-31G* level of theory in Gaussian 09 software. The vertical ionization potential (VIP) and vertical electron affinity (VEA) were calculated using the DFT at the single-point B3LYP/6-31+G(d,p) level of theory. No zero-point vibrational effects were included. The effect of bulk water as solvent was included through single-point calculations using the polarized continuum model (PCM) of Tomasi and coworkers.[5-7] The electronic ground state, the electronic excited state, and the spin-orbit coupling (SOC) constants of all molecules were obtained using time-dependent DFT (TD-DFT) at def2-TZVP/M06-2X level of theory in ORCA 4.1 (an *ab initio* quantum chemistry program). The electronic distribution of the frontier molecular orbitals (FMOs) was drawn using Gaussview 5.0.9.

Total reactive oxygen species (ROS) measurements. Prior to the measurements of total ROS, the chemical probe DCFH-DA was chemically activated to its deacetylated form 2',7'-dichlorofluorescin (DCFH) at a final concentration of 40 μM by referring to a previous study.[4] To the DCFH solution was added Azo-TPA-Th(+) (10 μM), TPA-Th(+) (10 μM; 20 μM), Azo-TPA(+) (10 μM), and TPA(+) (10 μM; 20 μM), respectively. The emission spectra (Ex = 488 nm) were then recorded at 10-second intervals under white light irradiation (380–800 nm) at a power density of 30 mW/cm^2, in which the DCFH solution was used as a control.

Type-II ROS measurements. ABDA was used as the indicator of singlet oxygen generation. To

eliminate the inner-filter effect, the absorption maxima of all photosensitizers were controlled at *ca.* 0.2. Briefly, 10 μL of ABDA stock solution (10 mM) was added to 2 mL of PBS with Azo-TPA-Th(+) (10 μM), TPA-Th(+) (10 μM; 20 μM), Azo-TPA(+) (10 μM), and TPA(+) (10 μM; 20 μM), respectively. After irradiation with white light (380−800 nm) at a power density of 30 mW/cm^2, the absorption spectra of ABDA were then recorded at 30-second intervals, and the absorbance at 378 nm was used as the variable parameter to calculate the decomposition rate of ABDA. The ABDA solution was used as a control.

Type-I ROS measurements. DHR-123 was used as the indicator of the generation of superoxide anion radicals by converting into the fluorescent rhodamine 123. Briefly, 10 μL of DHR-123 stock solution (10 mM) was added to 2 mL of PBS with Azo-TPA-Th(+) (10 μM), TPA-Th(+) (10 μM; 20 μM), Azo-TPA (+) (10 μM), and TPA(+) (10 μM; 20 μM), respectively. After irradiation with white light at a power density of 30 mW/cm^2, the emission spectra of DHR-123 (Ex = 488 nm) were then recorded at 30-second intervals, and the emission intensity at 525 nm was used as the variable parameter to calculate the conversion rate of DHR-123. In terms of the quenching of superoxide anion radicals, Vc was added to the aforementioned systems at a final concentration of 50 μM prior to white light irradiation. The DHR-123 solution was used as a control.

Electron spin resonance (ESR) spectroscopy. The ESR measurements were carried out on a Bruker Model E580-10/12 EPR spectrometer at ambient temperature. The spin trapping agent 5,5-dimethyl-1-pyrroline-N-oxide (DMPO, 100 mM) was used to trap the generated radicals, in which the Azo-TPA-Th(+) in PBS (100 μM) was irradiated for 10 min under white light at power density of 30 mW/cm^2.

Bacterial culture. Methicillin-resistant *Staphylococcus aureus* (MRSA) was provided by Prof. Jianfeng Liu (Institute of Radiation Medicine, Chinese Academy of Medical Sciences and Peking Union Medical College, Tianjin, China). For bacterial culture, 5 mL of Tryptic Soy Broth (TSB)

with 10 μg/mL tetracycline hydrochloride was inoculated with a single colony of MRSA on a solid TSB agar plate and grown at 37 °C overnight in a shaking incubator at 170 rpm. The bacterial cultures were collected by centrifugation at 3500 *g* for 3 min, followed by washing with PBS. The supernatant was discarded, and the remaining bacteria were resuspended in PBS. The bacterial suspension was further adjusted with PBS to an optical density of 0.5 at 600 nm (OD_{600} = 0.5) for subsequent use.

In vitro antibacterial experiments of Azo-TPA-Th(+). The bacterial suspensions (MRSA, OD_{600} = 0.5, 200 μL) were mixed with Azo-TPA-Th(+) at final concentrations of (0, 0.625, 1.25, 2.5, 5, and 10 μM), followed by adding into a 24-well plate and incubating in the dark at 37 °C for 10 min. Next, the bacteria treated with Azo-TPA-Th(+) were irradiated by white light at a power density of 40 mW/cm^2 for 5 min or placed in the dark for 5 min. The treated bacterial suspensions were then diluted by 5 × 10^3 fold with PBS, and 100 μL of the diluted bacterial solutions were spread on TSB agar plates with 10 μg/mL tetracycline hydrochloride, followed by culturing at 37 °C for 18–20 h. The colony-forming units (CFU) of each plate were then counted for quantitative antibacterial analysis (*n* = 3).

Live/dead staining assay. Live/Dead®Baclight™ bacterial viability kit was used to differentiate the viability of bacteria, in which bacteria with intact cell membranes emitted green fluorescence, whereas bacteria with damaged cell membranes emitted red fluorescence. Specifically, the bacterial suspensions (OD_{600} = 0.5, 200 μL) were mixed with Azo-TPA-Th(+) at a final concentration of 5 μM, followed by adding into a 24-well plate and incubating in the dark at 37 °C for 10 min. For the irradiated group, the bacterial suspension was exposed to white light irradiation at a power density of 40 mW/cm^2 for 5 min. For comparisons, three control groups were prepared, including the bacteria treated with PBS with and without light irradiation as well as the bacteria treated with Azo-TPA-Th(+) (5 μM) without light irradiation. The bacteria were then collected by centrifugation at 3500 *g* for 3 min and washed with PBS, followed by staining with SYTO 9 (3.34

μM) and propidium iodide (PI, 30 μM) for 15 min in the dark. The bacterial suspensions (10 μL) were added to glass slide, which were carefully covered by a clean coverslip for characterization by a confocal laser scanning microscope (CLSM, $A1^+$, Nikon; SYTO 9, Ex = 488 nm, Em = 490−540 nm; PI, Ex = 488 nm, Em = 630−680 nm).

Scanning electron microscopy (SEM) analysis. Once the incubation was completed as described in "***Live/dead staining assay***", the bacteria were collected by centrifugation at 3500 *g* for 3 min, washed with PBS, and fixed with 2.5% glutaraldehyde at ambient temperature for 30 min. The mixture was then centrifuged at 3500 *g* for 10 min, washed with PBS, and resuspended in water (20 μL). The bacterial suspensions (5 μL) were placed on clean silicon wafers, followed by air drying. Immediately after the samples became dried, the silicon wafers were immersed in 2.5% glutaraldehyde and fixed at ambient temperature overnight. Subsequently, the samples were washed with water twice and subjected to gradient ethanol dehydration from 30% to 100% (including 30%, 50%, 70%, 80%, 90%, and 100%, 6 min × 2 times for each concentration). After the samples were fully dried, they were coated with gold before examination under a scanning electron microscope (SEM; JSM-7500F, JEOL).

Responsiveness of Azo-TPA-Th(+) to UV light irradiation. The absorption and emission spectra (Ex = 385 nm) of Azo-TPA-Th(+) (20 μM) in PBS were measured post-irradiation with a 365 nm UV light at a power density of 180 mW/cm^2 for different periods of time (0, 5, 10, 15, and 30 min). The ROS generation capacity of Azo-TPA-Th(+) post UV irradiation was evaluated using the identical procedure as described in the section of "***Type-II ROS measurements***". The particle size distribution and the morphology of Azo-TPA-Th(+) aggregates before and after UV irradiation were characterized by DLS and transmission electron microscopy (TEM; JEM-1400 FLASH, JEOL), respectively. In addition, the emission spectra of bacterial suspensions (OD_{600} = 0.1, 0.25, 0.5, 0.75, and 1.0) mixed with Azo-TPA-Th(+) (5 μM) were recorded after irradiation with a 365 nm UV light at a power density of 180 mW/cm^2 for different periods of time (0, 5, 10, 15, and 30

min).

References

1. Z. Yang, W. Yin, S. Zhang, I. Shah, B. Zhang, S. Zhang, Z. Li., Z. Lei. and H. Ma, *ACS Appl. Bio Mater.*, 2020, **3**, 1187–1196.
2. Y. Hayashi, N. Suzuki, T. Maeda, H. Fujiwarab and S. Yag, *New J. Chem*., 2021, **45**, 9770–9779.
3. J. Sivamani, R. Balasaravanan, K. Duraimurugan and A. Siva, *Photochem. Photobiol. Sci.*, 2016, **15**, 211–218.
4. L. Bourré, S. Thibaut, A. Briffaud, N. Rousset, S. Eléouet, Y. Lajat and T. Patrice, *J. Photochem. Photobiol. B*, 2002, **67**, 23–31.
5. S. Miertuš, E. Scrocco and J. Tomasi, *Chem. Phys.*, 1981, **55**, 117–129.
6. S. Miertuš and J. Tomasi, *Chem. Phys.* 1982, **65**, 239–245.
7. M. Cossi, V. Barone, R. Cammi and J. Tomasi, *Chem. Phys. Lett.*, 1996, **255**, 327–335.

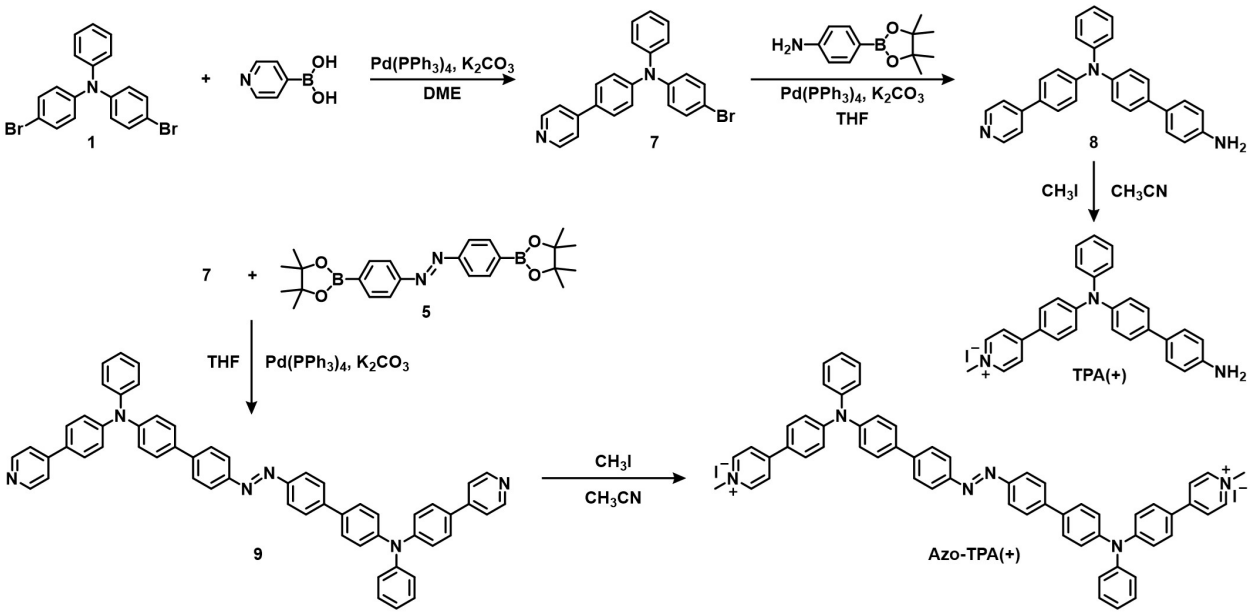

Scheme S1. Synthetic routes to TPA(+) and Azo-TPA(+).

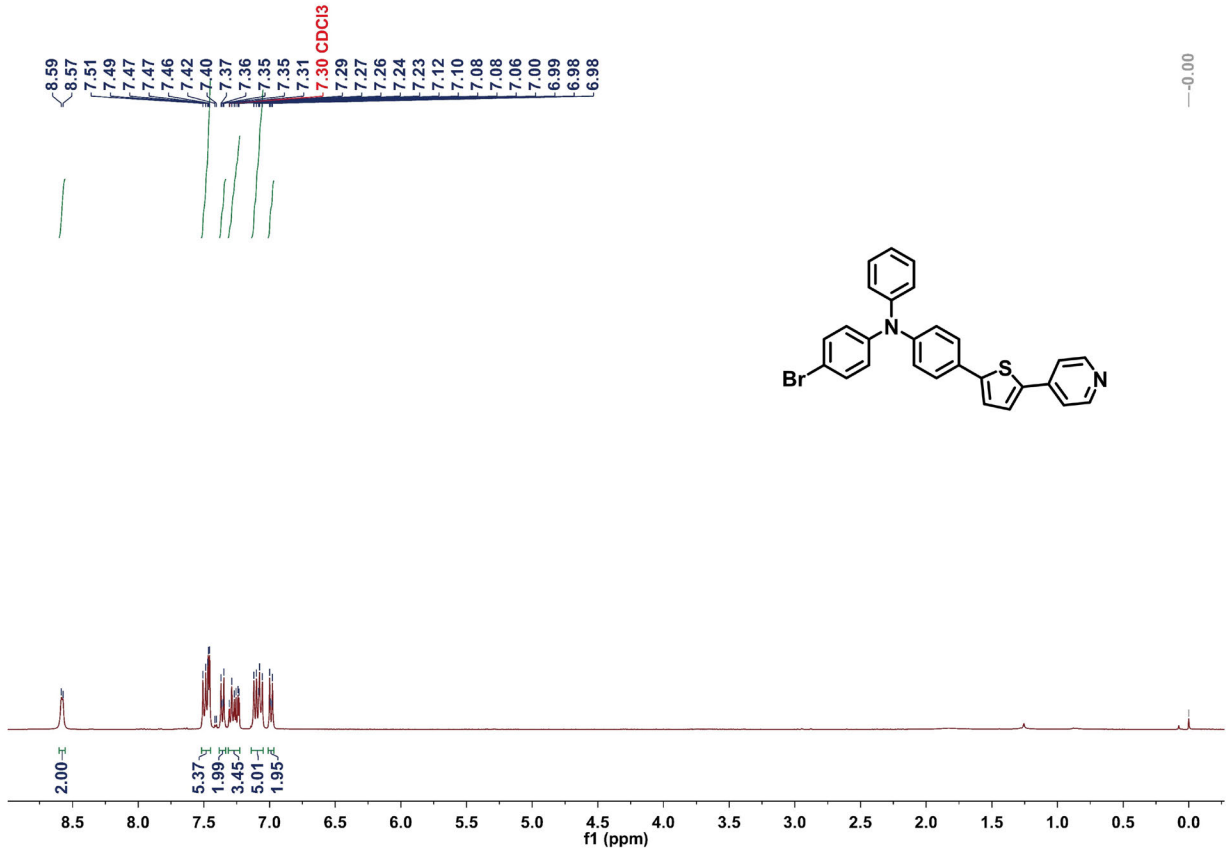

Figure S1. ^{1}H-NMR spectrum of compound **3** in $CDCl_3$.

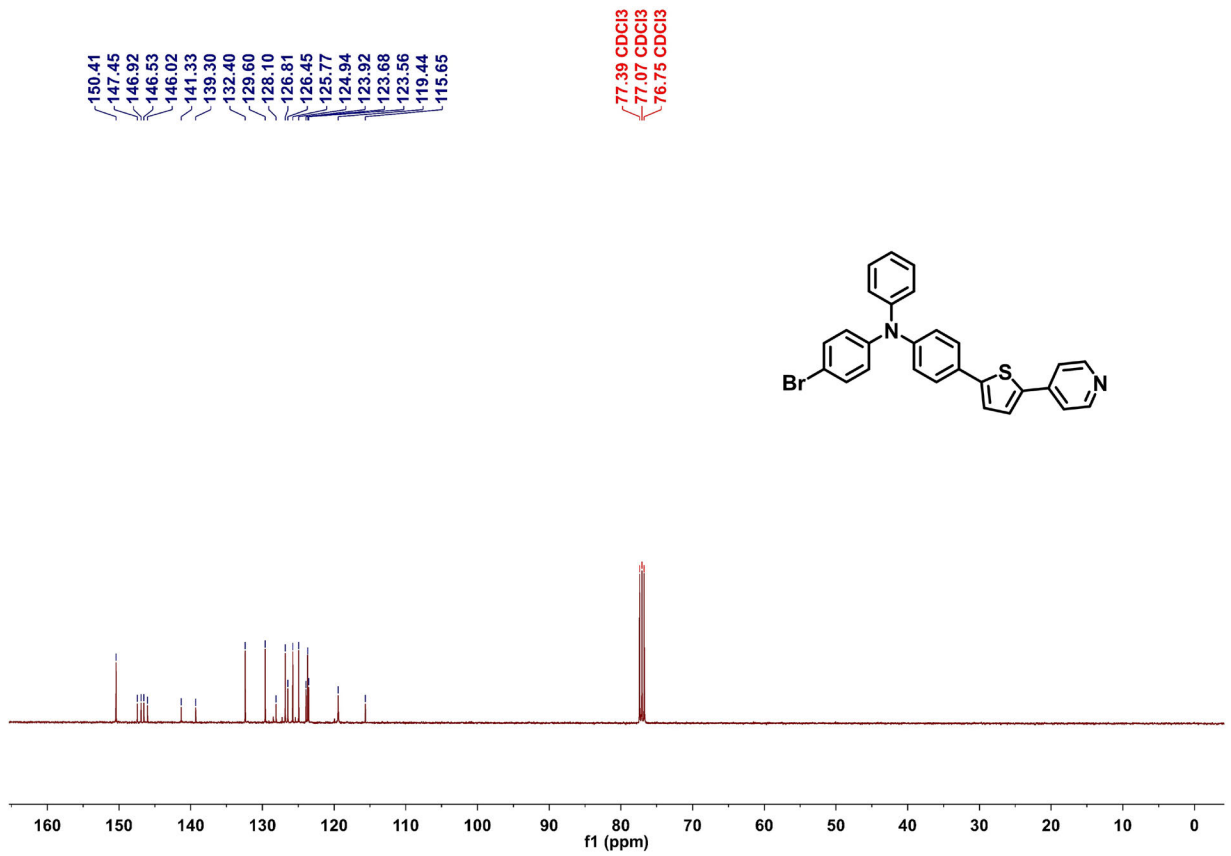

Figure S2. ^{13}C-NMR spectrum of compound **3** in $CDCl_3$.

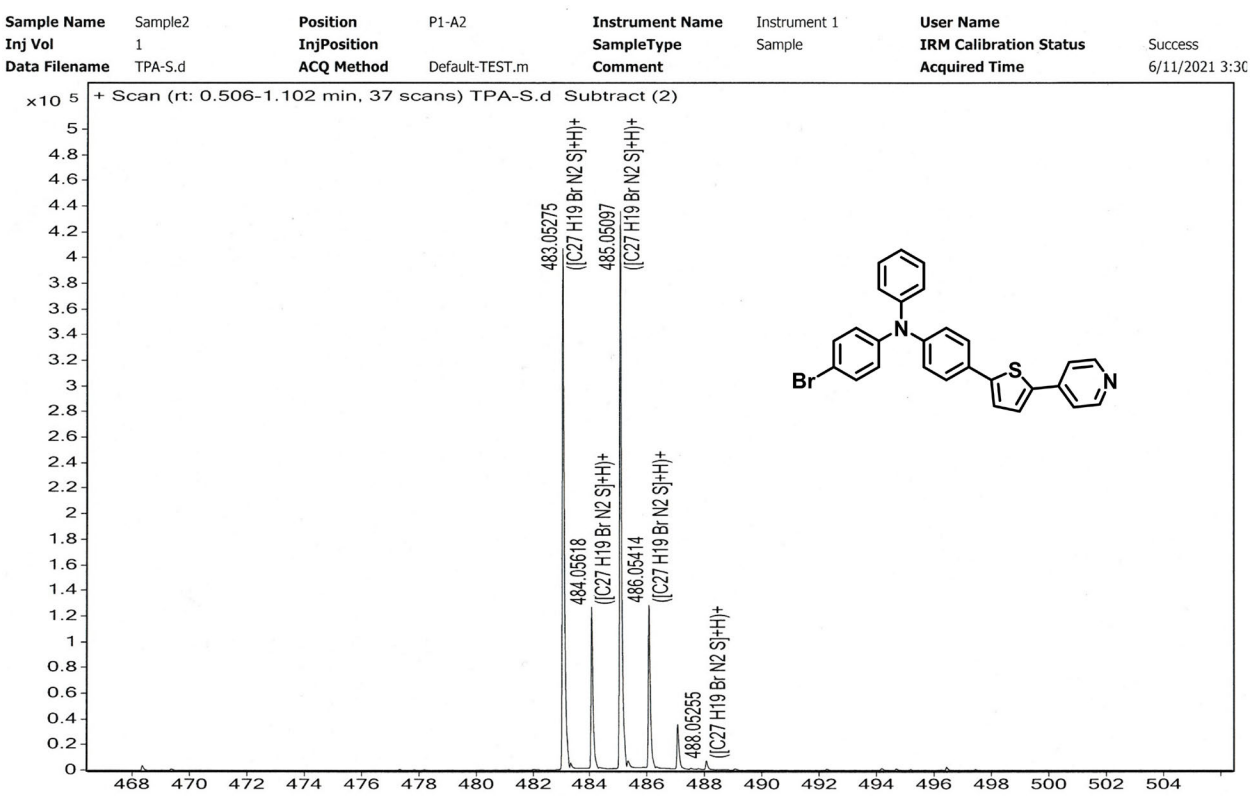

Figure S3. HRMS spectrum of compound **3**.

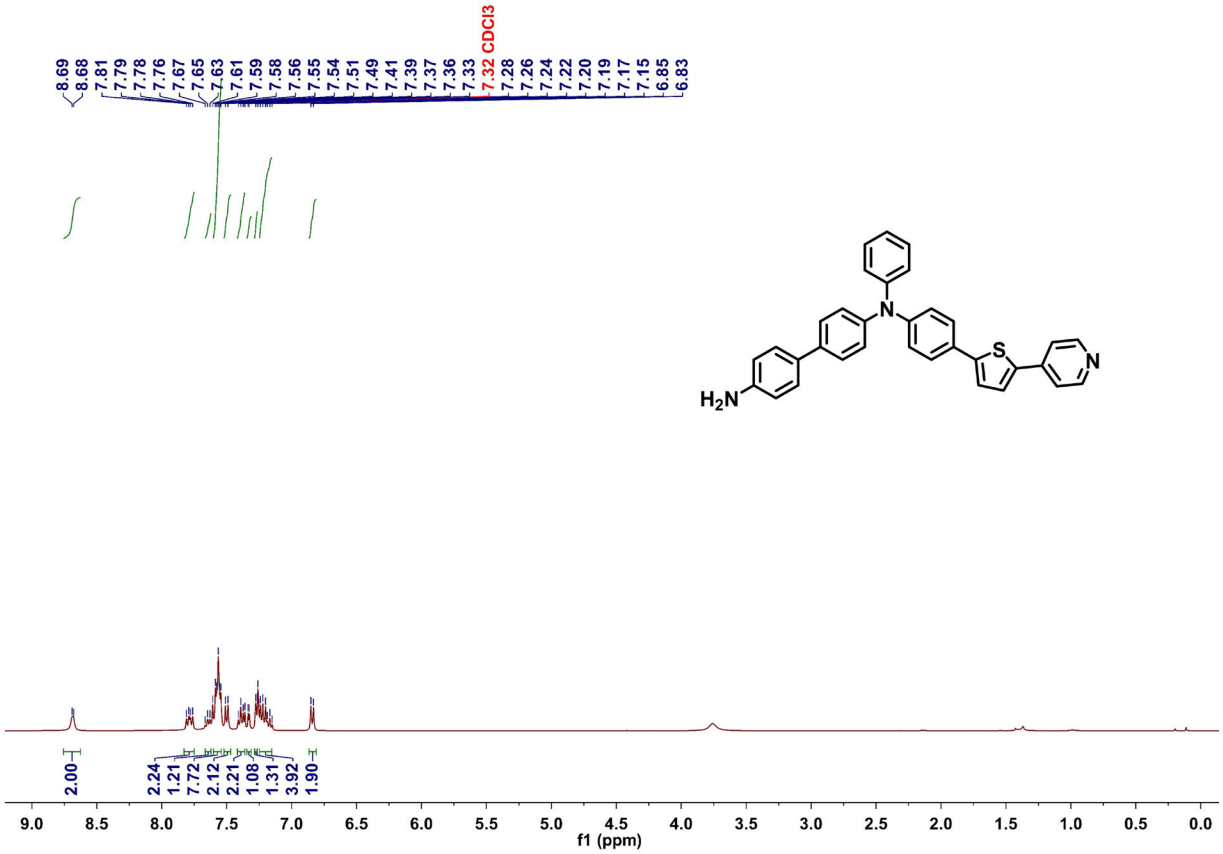

Figure S4. ^{1}H-NMR spectrum of compound **4** in $CDCl_3$.

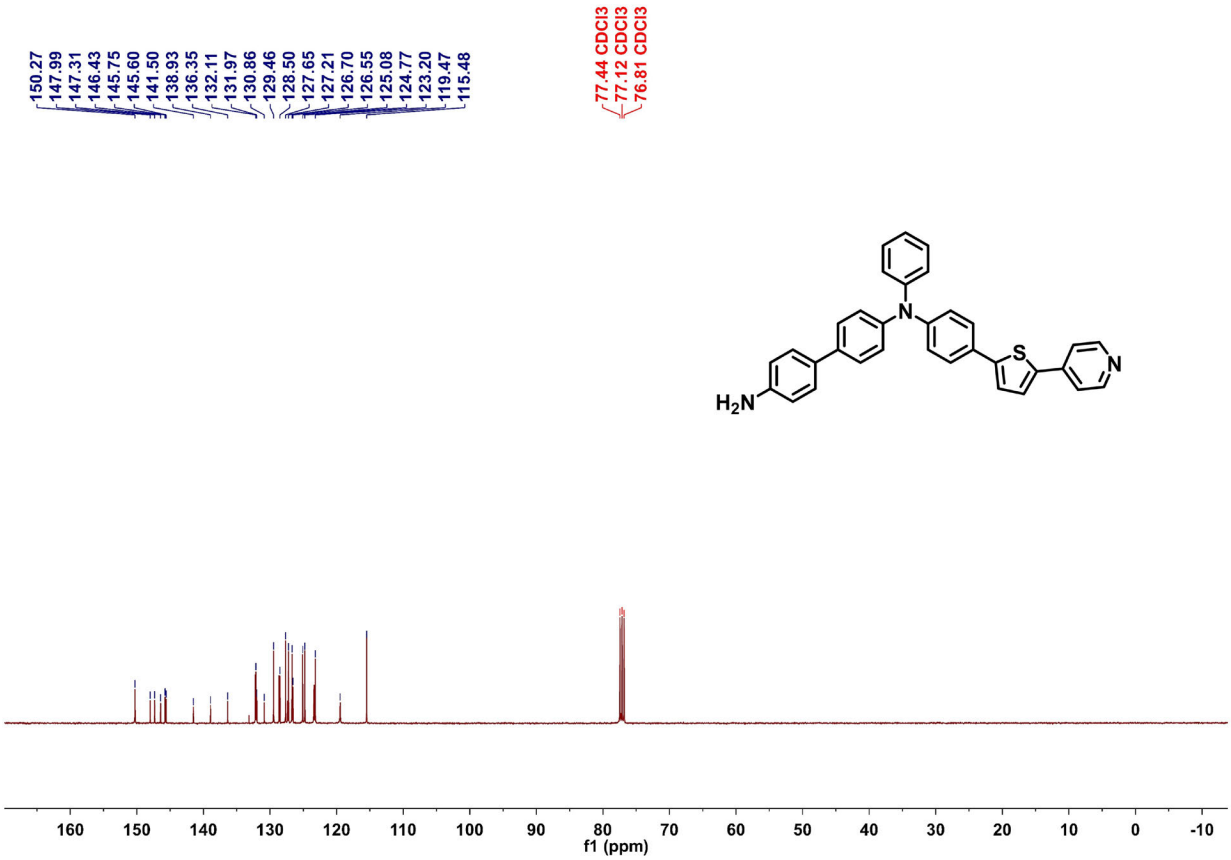

Figure S5. ^{13}C-NMR spectrum of compound **4** in $CDCl_3$.

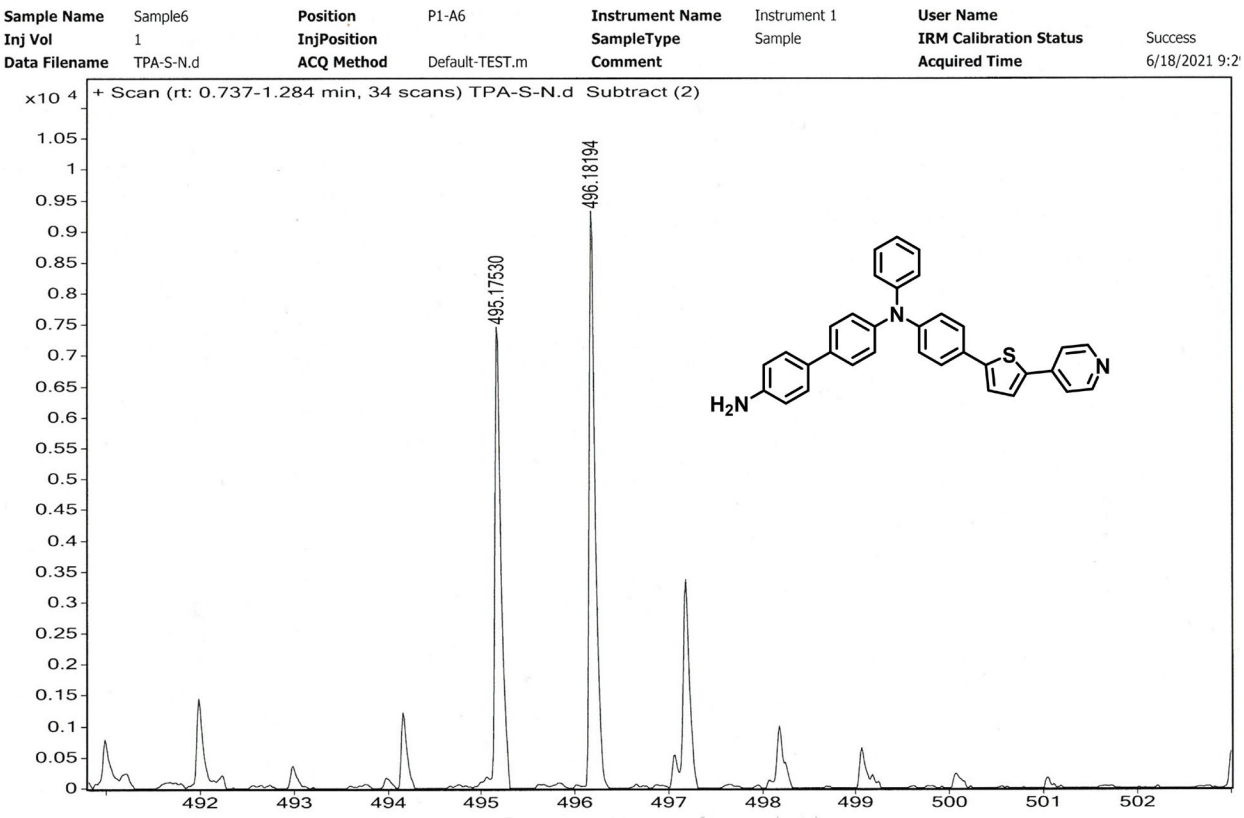

Figure S6. HRMS spectrum of compound **4**.

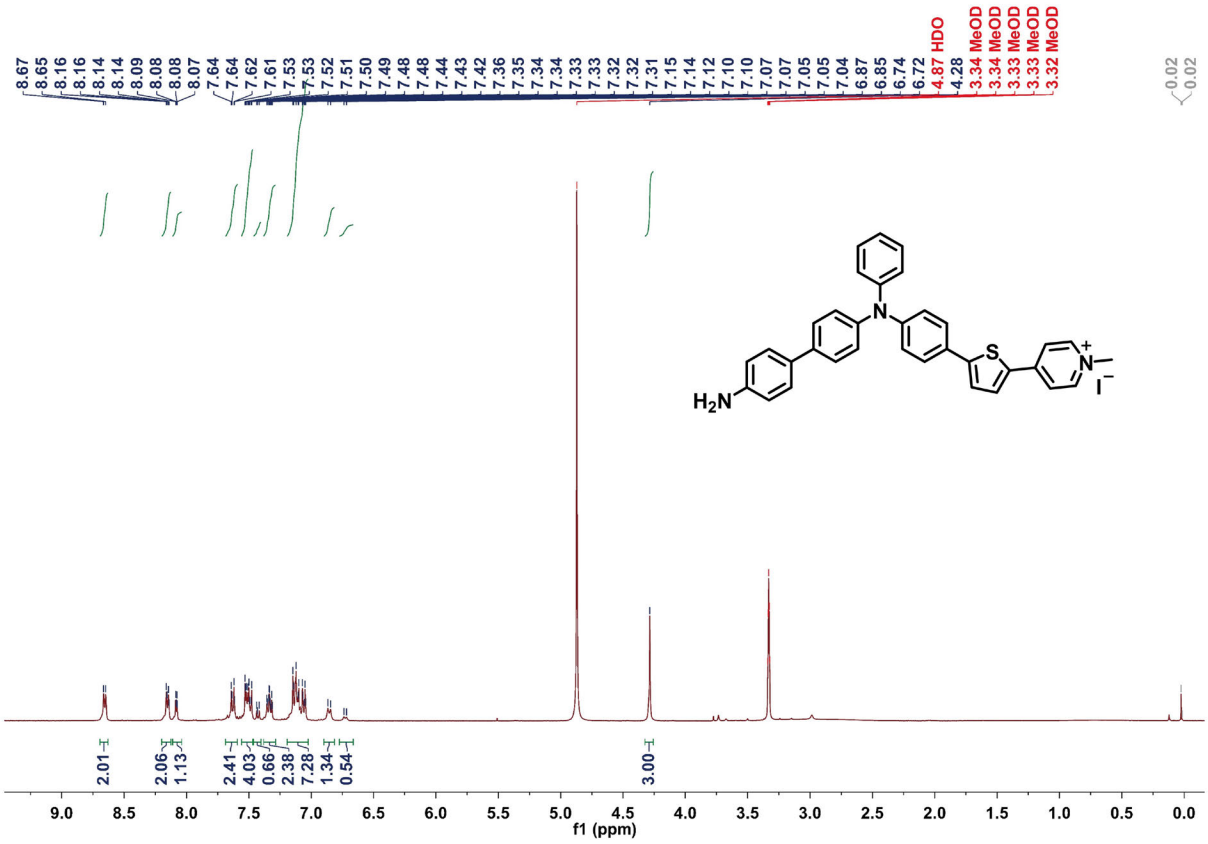

Figure S7. ^{1}H-NMR spectrum of TPA-Th(+) in CD_3OD.

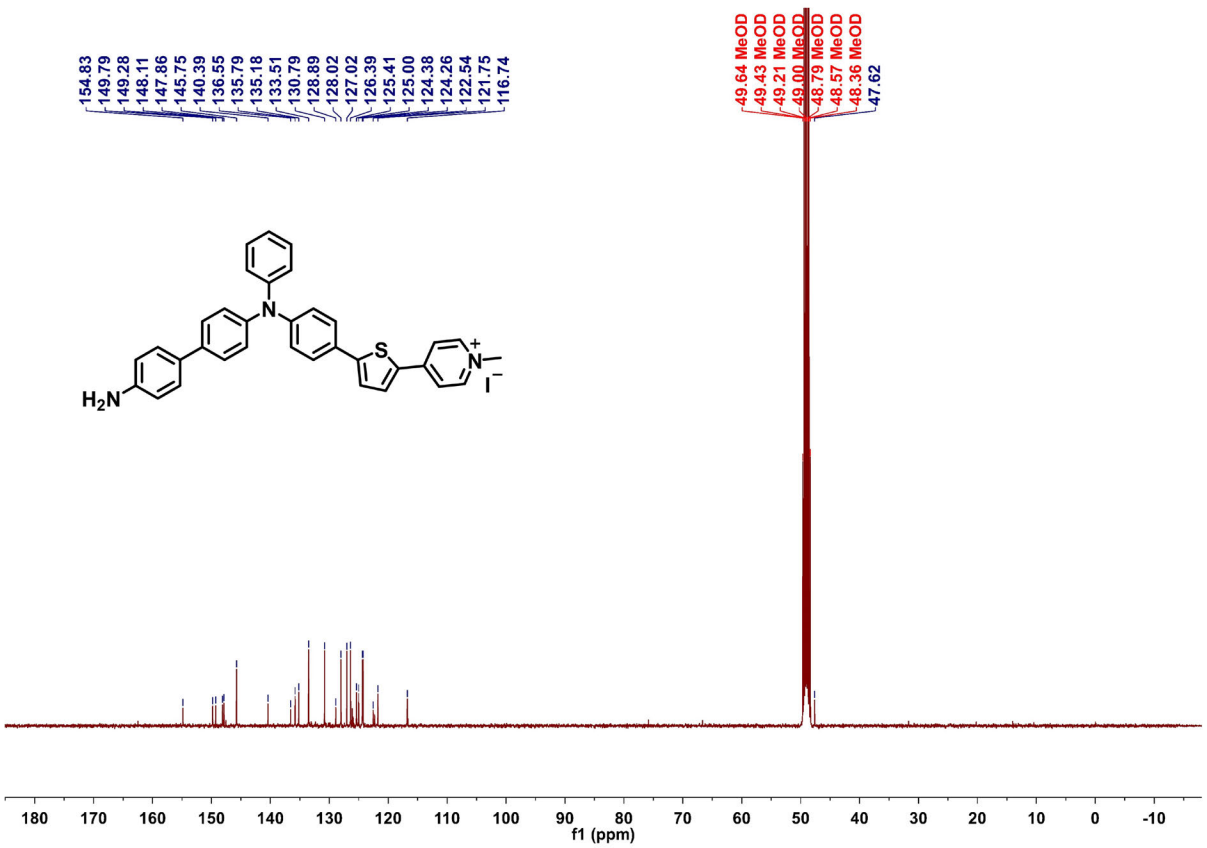

Figure S8. ^{13}C-NMR spectrum of TPA-Th(+) in CD_3OD.

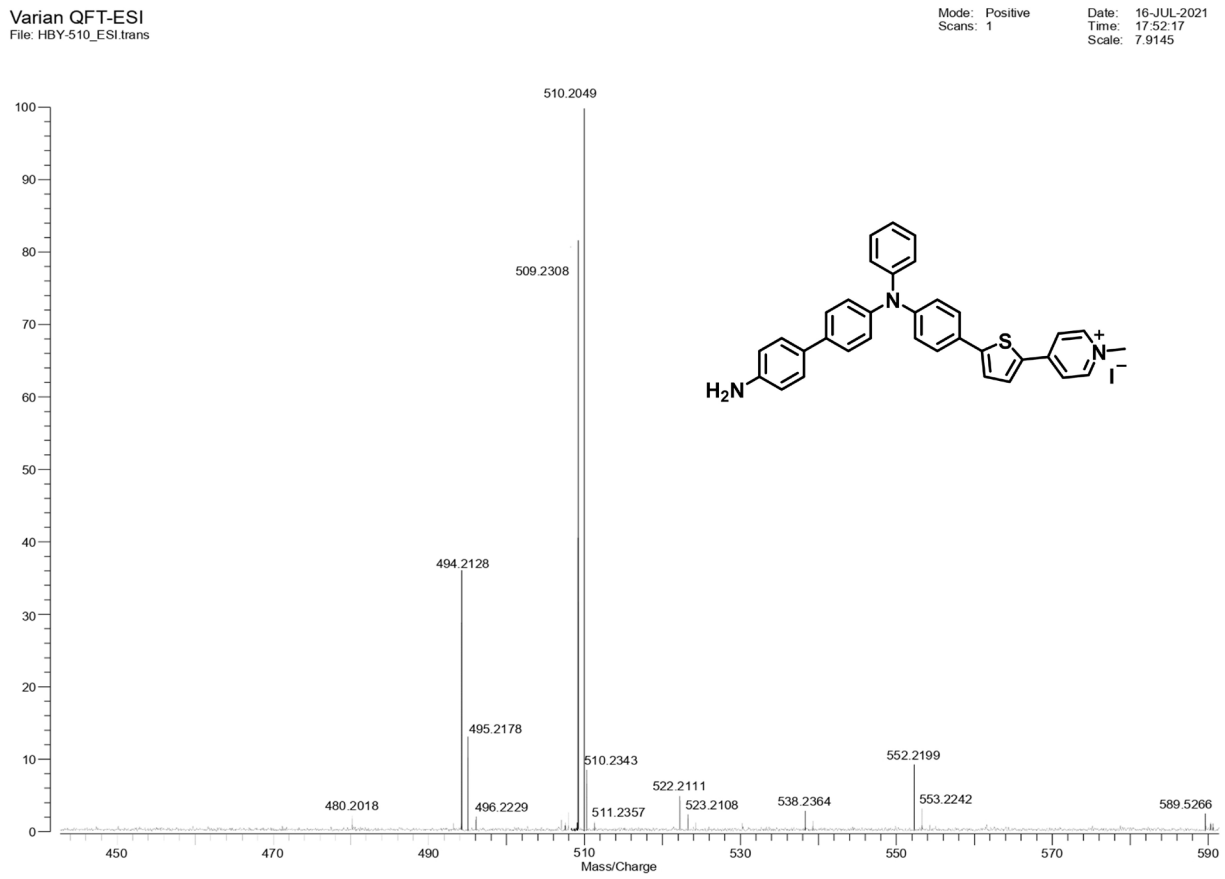

Figure S9. HRMS spectrum of TPA-Th(+).

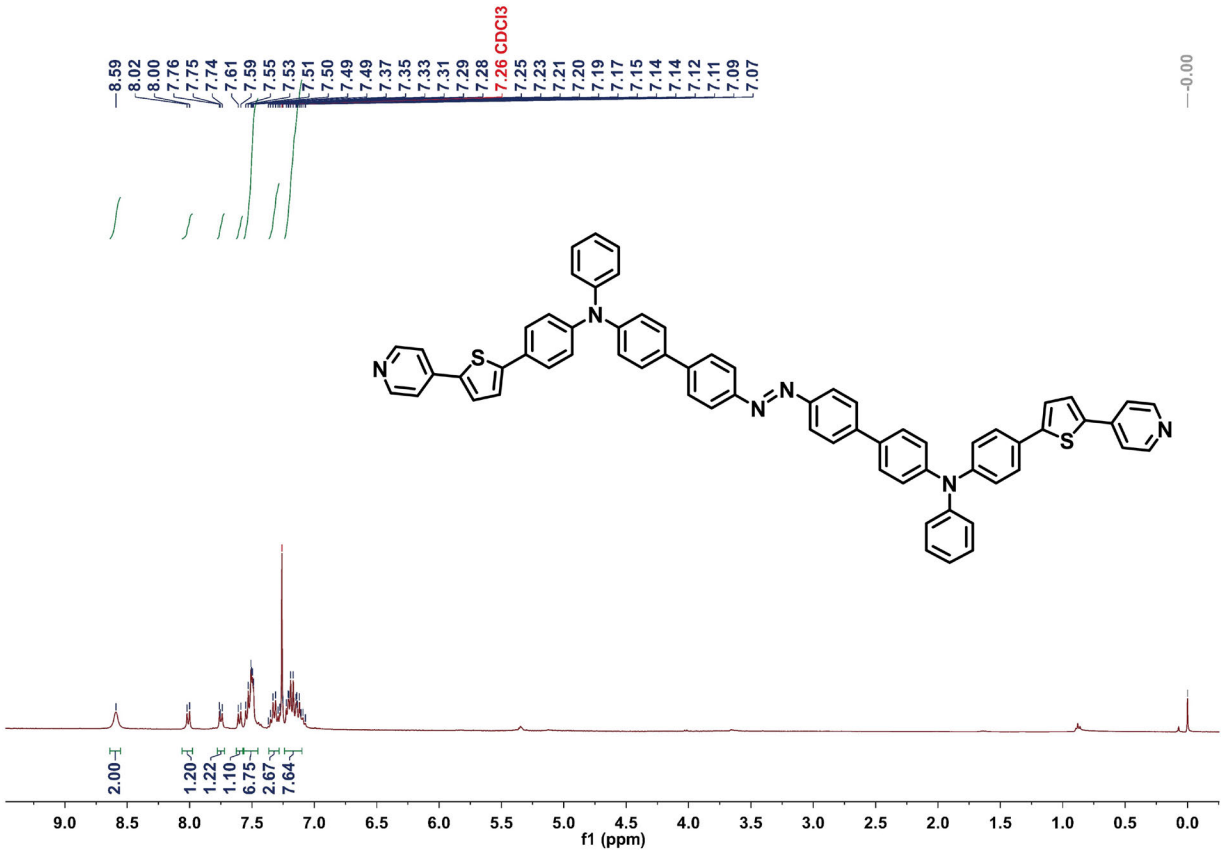

Figure S10. ^{1}H-NMR spectrum of compound **6** in $CDCl_3$.

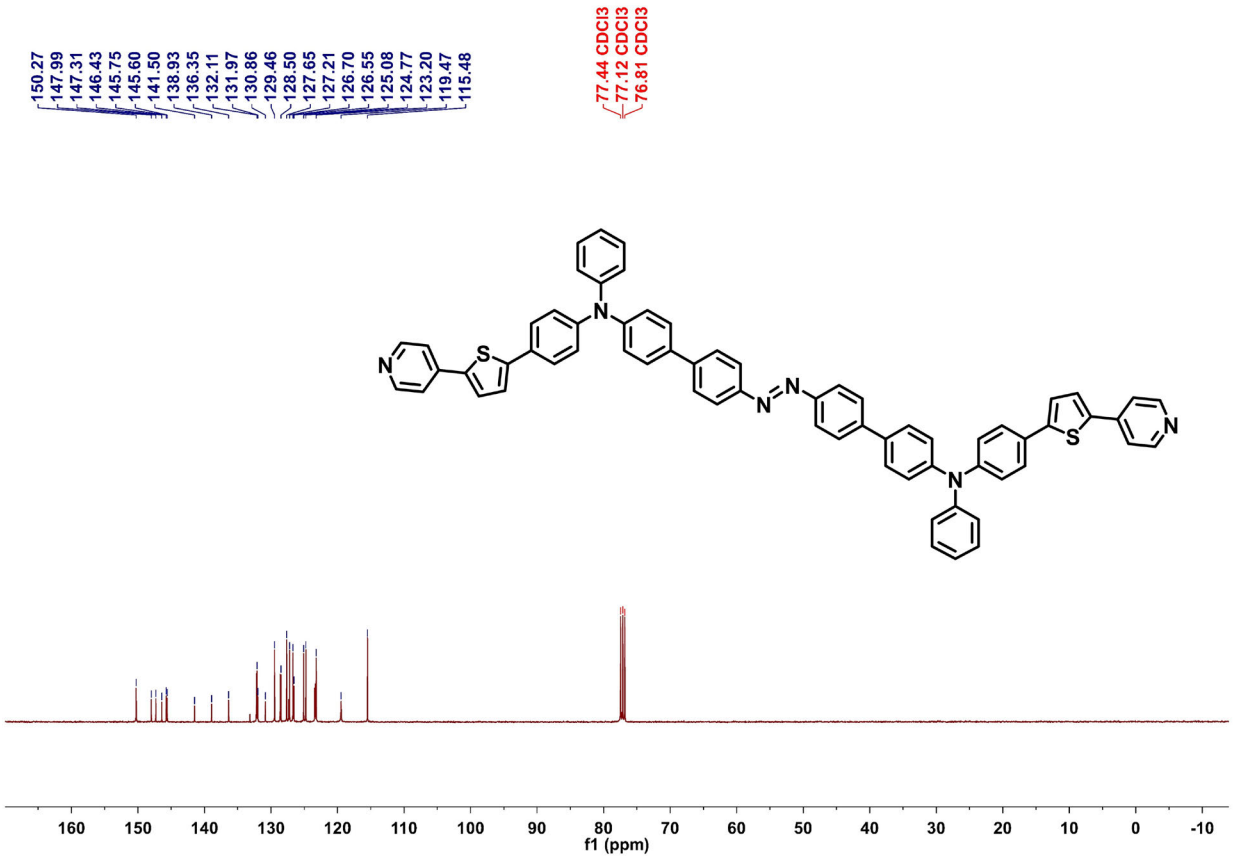

Figure S11. ^{13}C-NMR spectrum of compound **6** in $CDCl_3$.

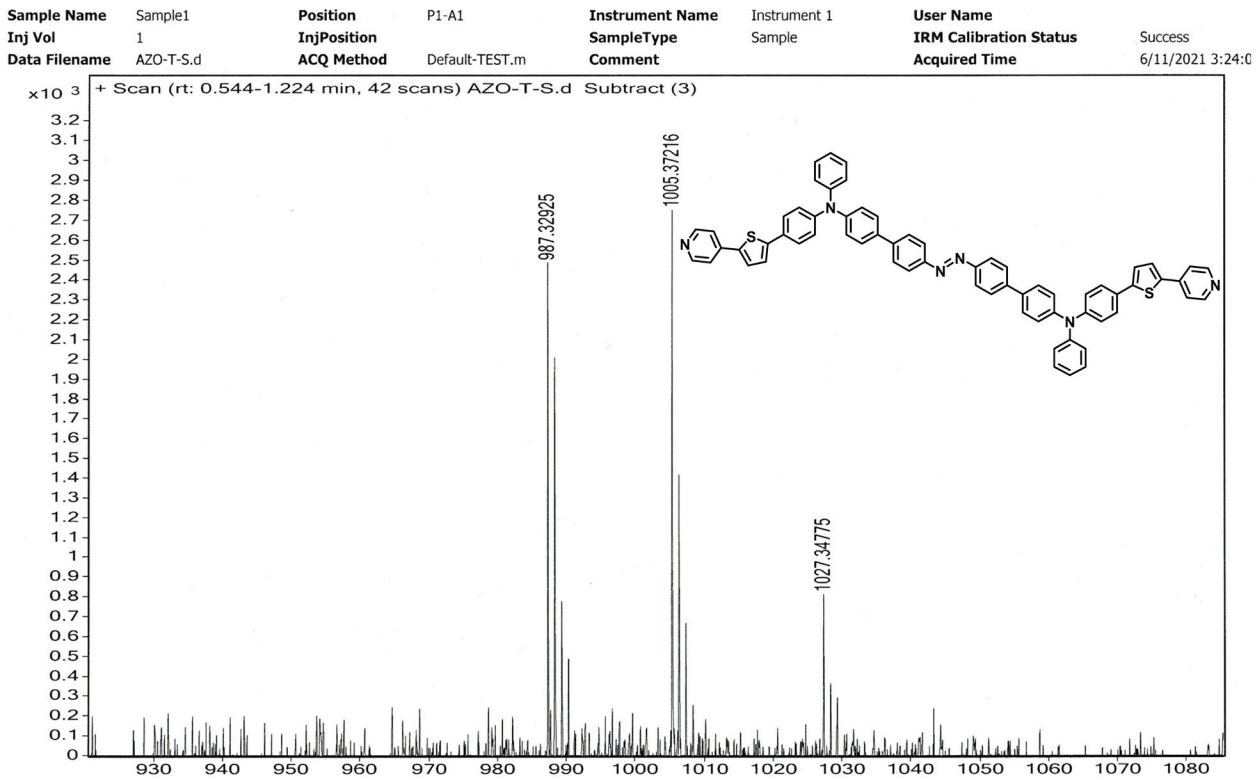

Figure S12. HRMS spectrum of compound **6**.

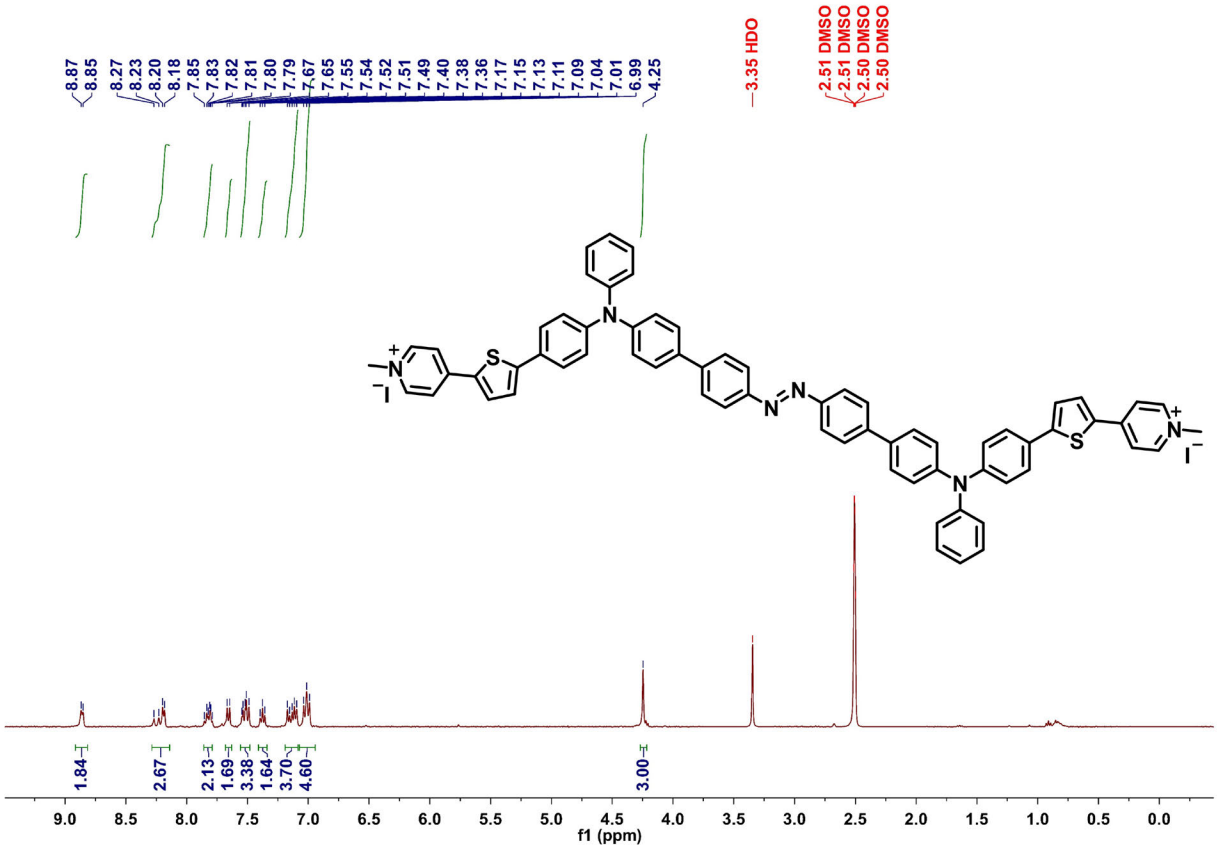

Figure S13. ^{1}H-NMR spectrum of Azo-TPA-Th(+) in DMSO-d_6.

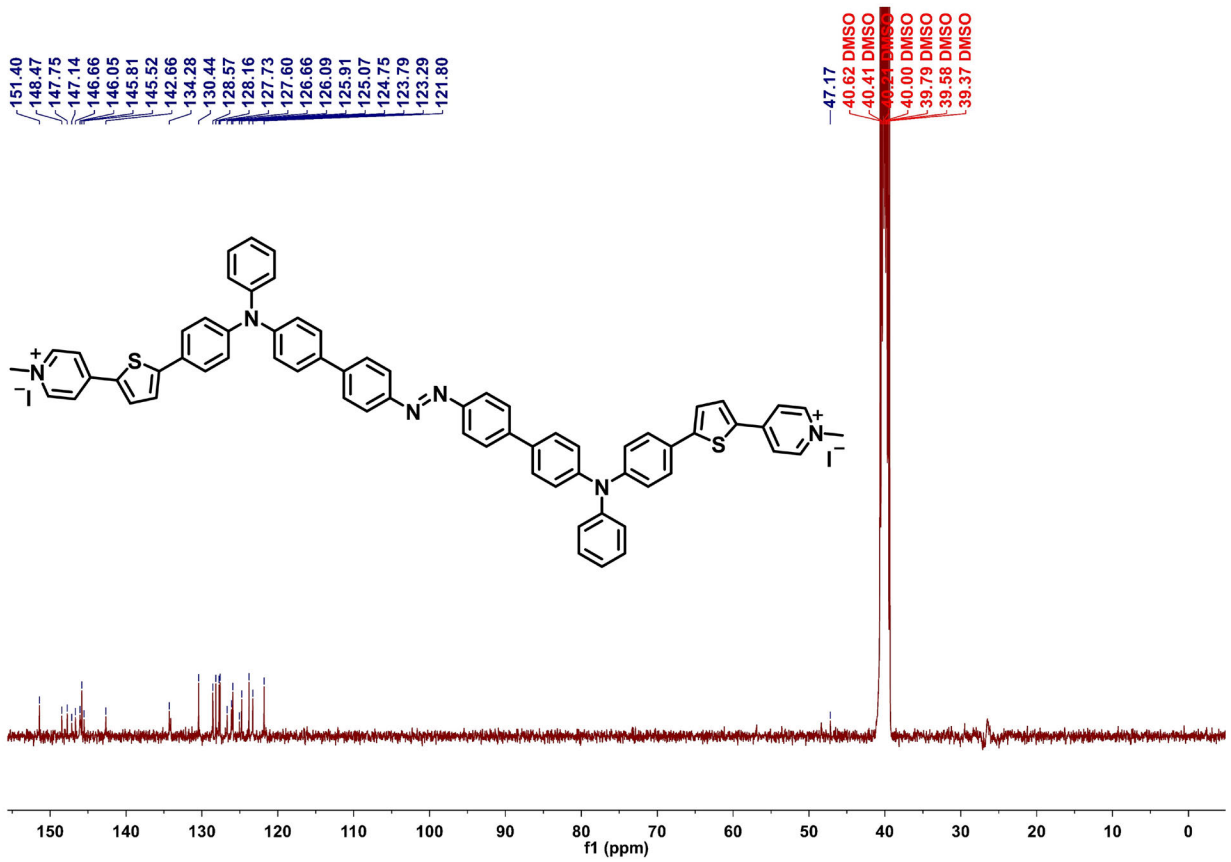

Figure S14. ^{13}C-NMR spectrum of Azo-TPA-Th(+) in DMSO-d_6.

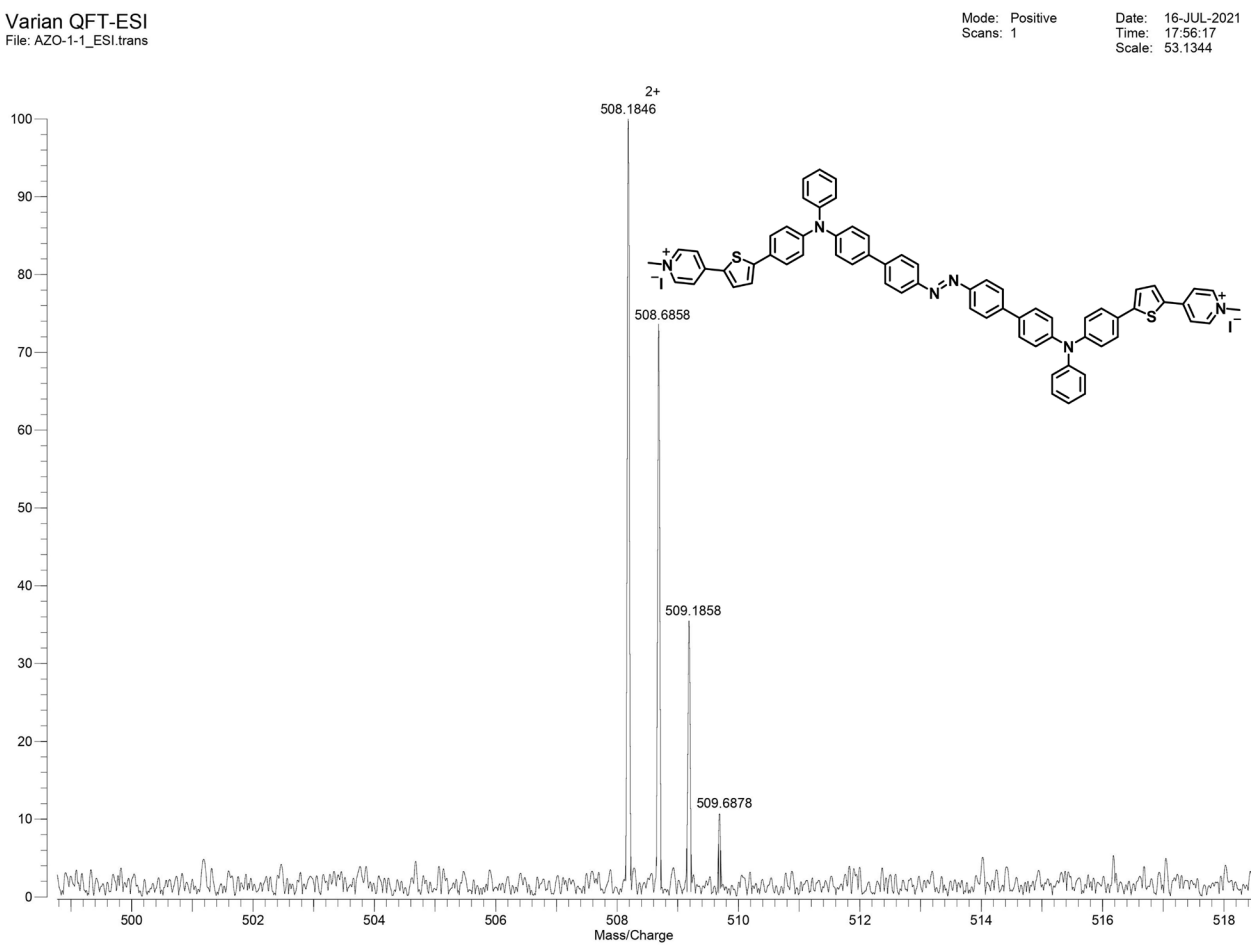

Figure S15. HRMS spectrum of Azo-TPA-Th(+).

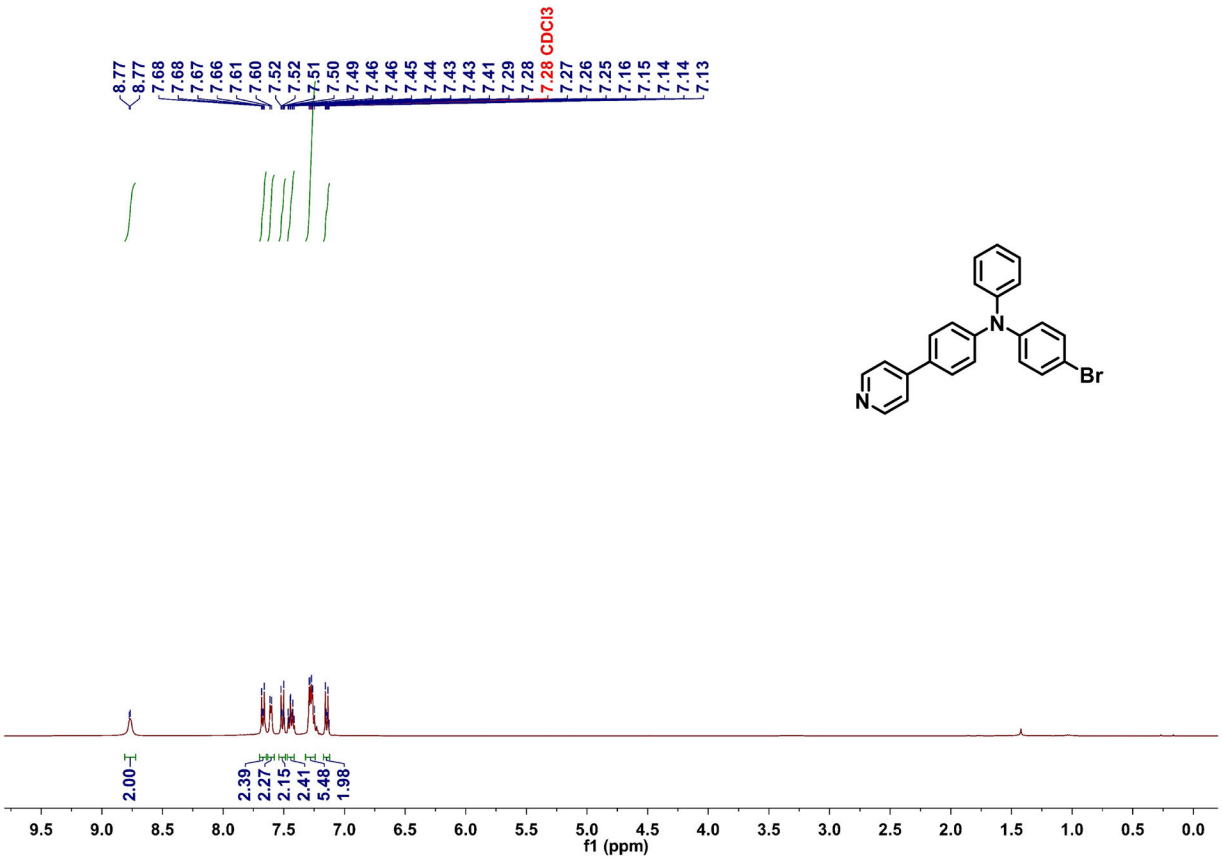

Figure S16. ^{1}H-NMR spectrum of compound **7** in $CDCl_3$.

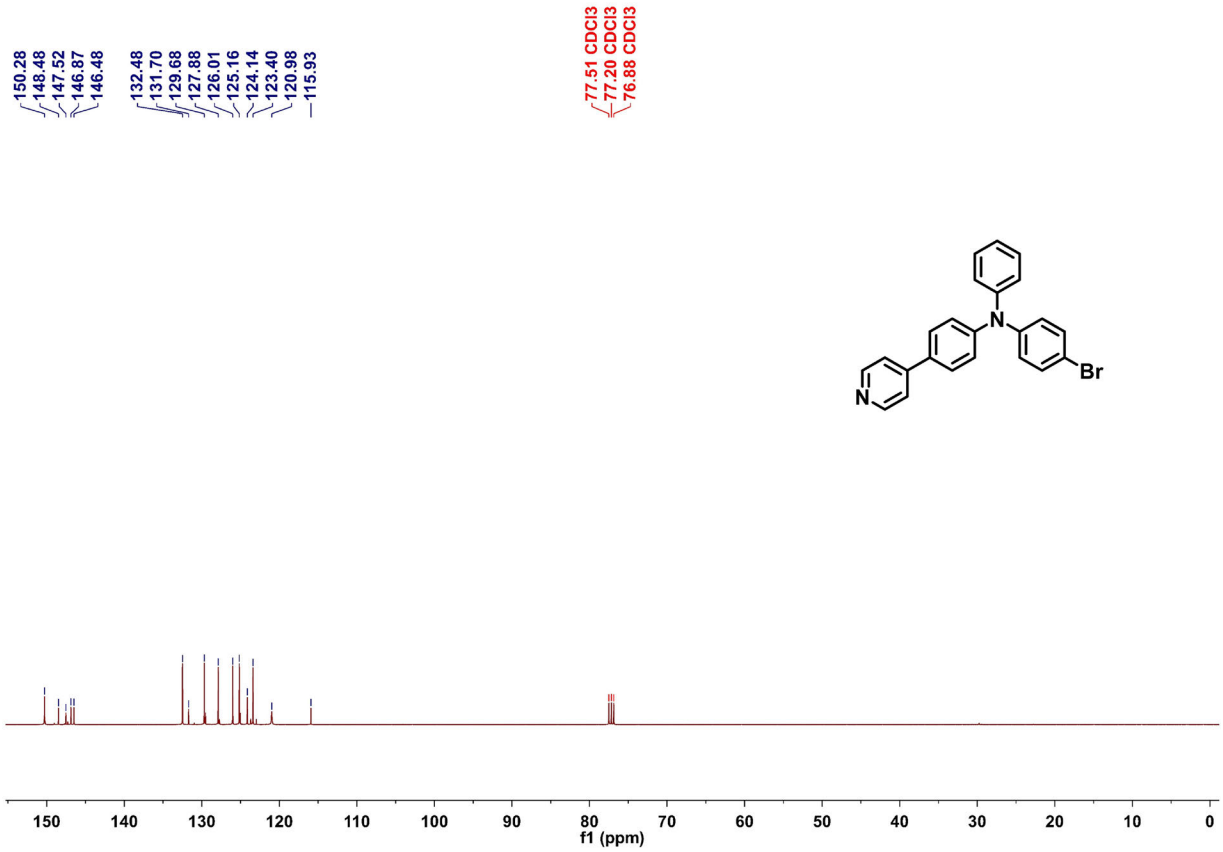

Figure S17. ^{13}C-NMR spectrum of compound **7** in $CDCl_3$.

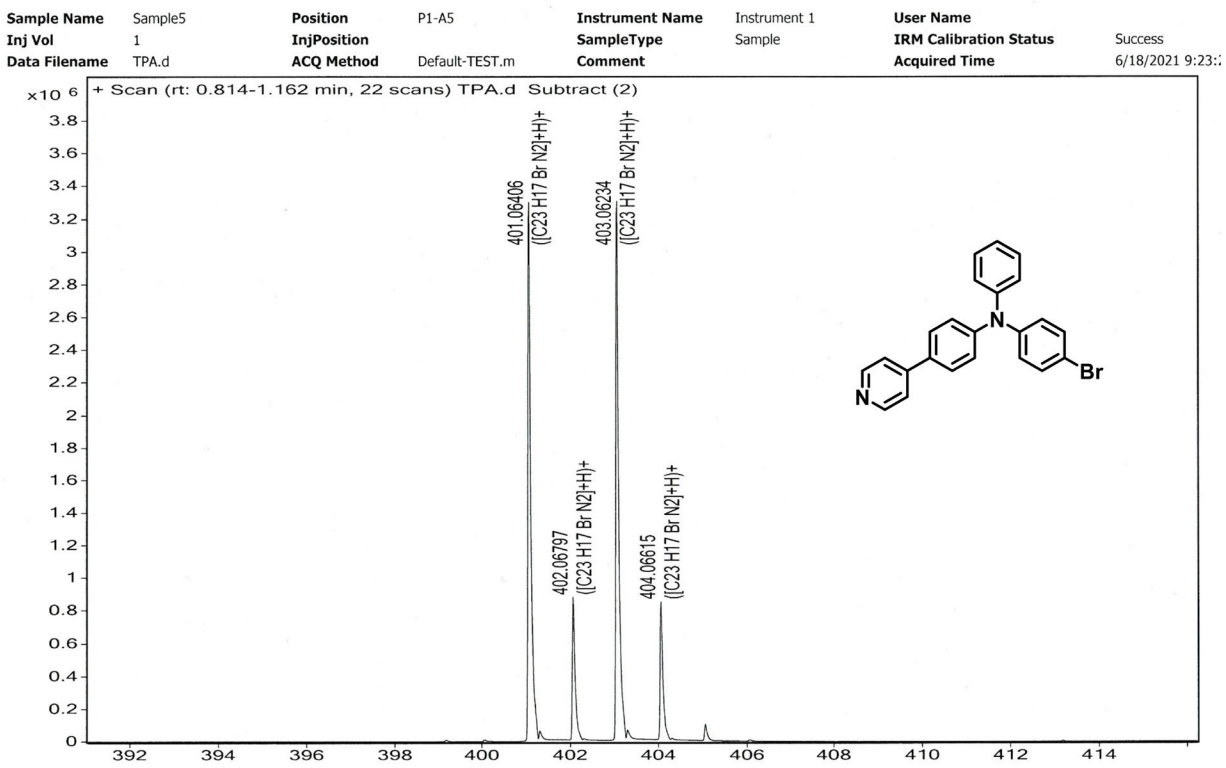

Figure S18. HRMS spectrum of compound **7**.

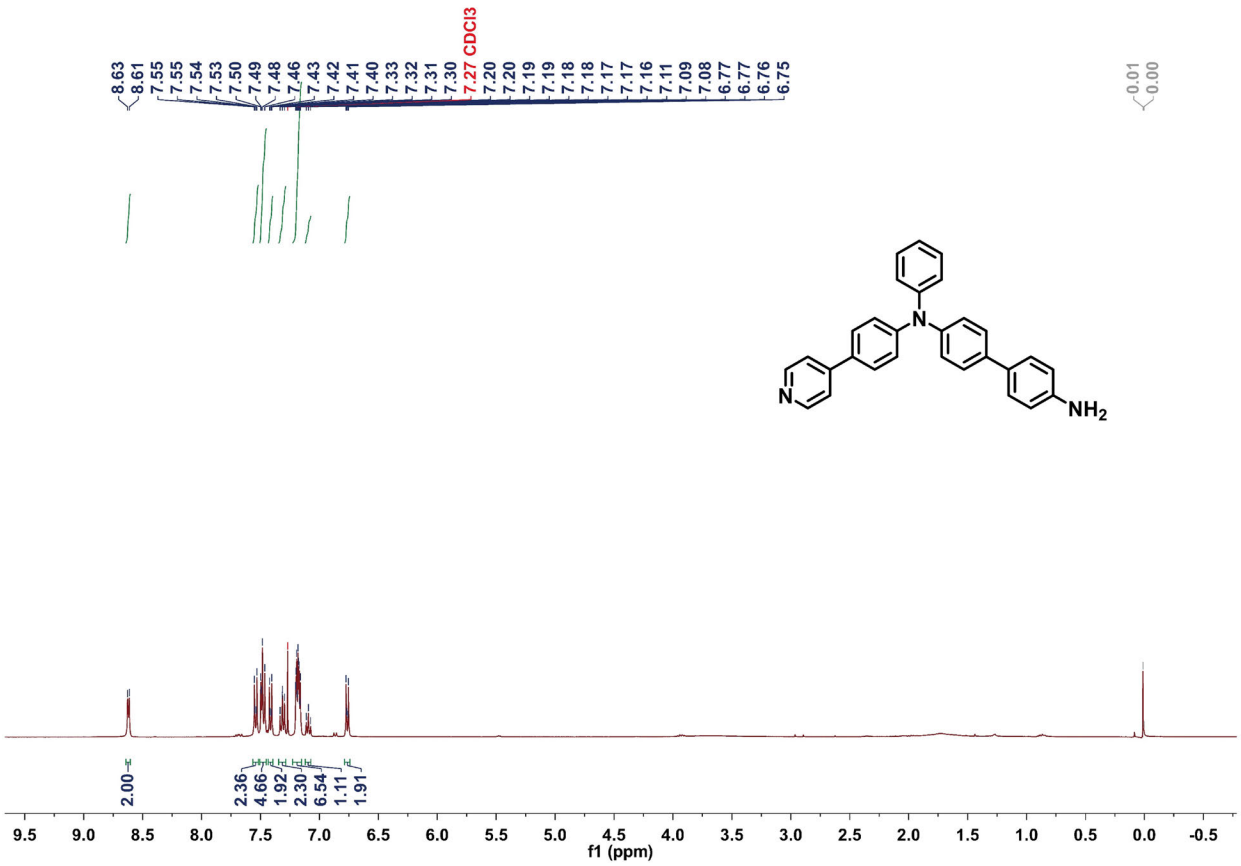

Figure S19. ^{1}H-NMR spectrum of compound **8** in $CDCl_3$.

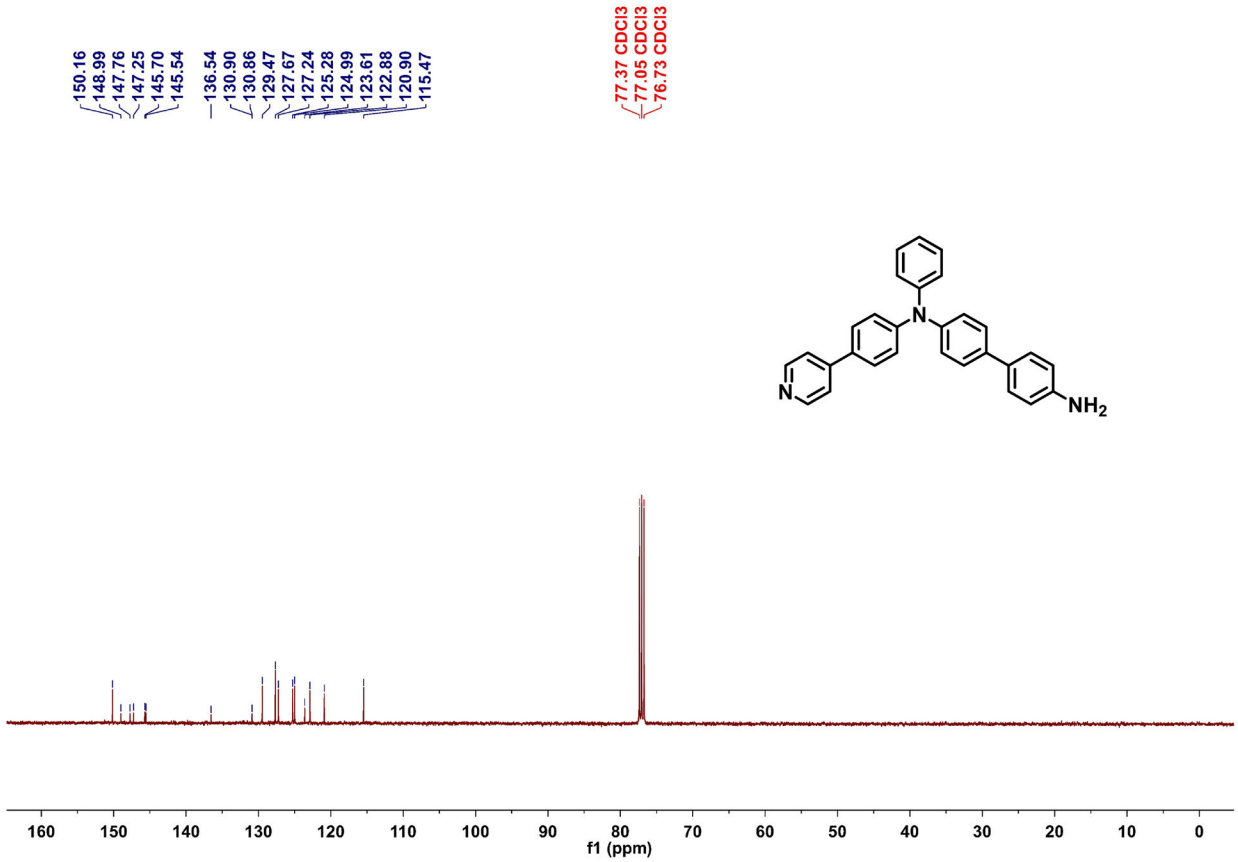

Figure S20. ^{13}C-NMR spectrum of compound **8** in $CDCl_3$.

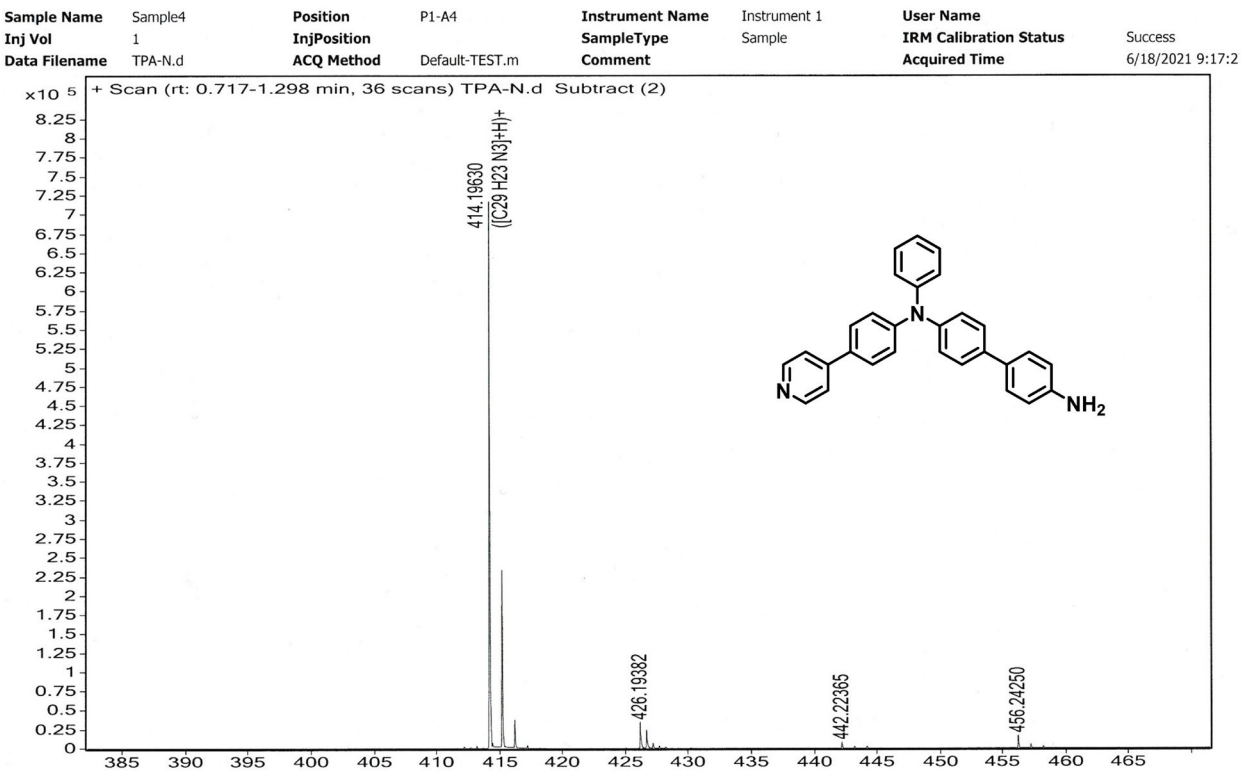

Figure S21. HRMS spectrum of compound **8**.

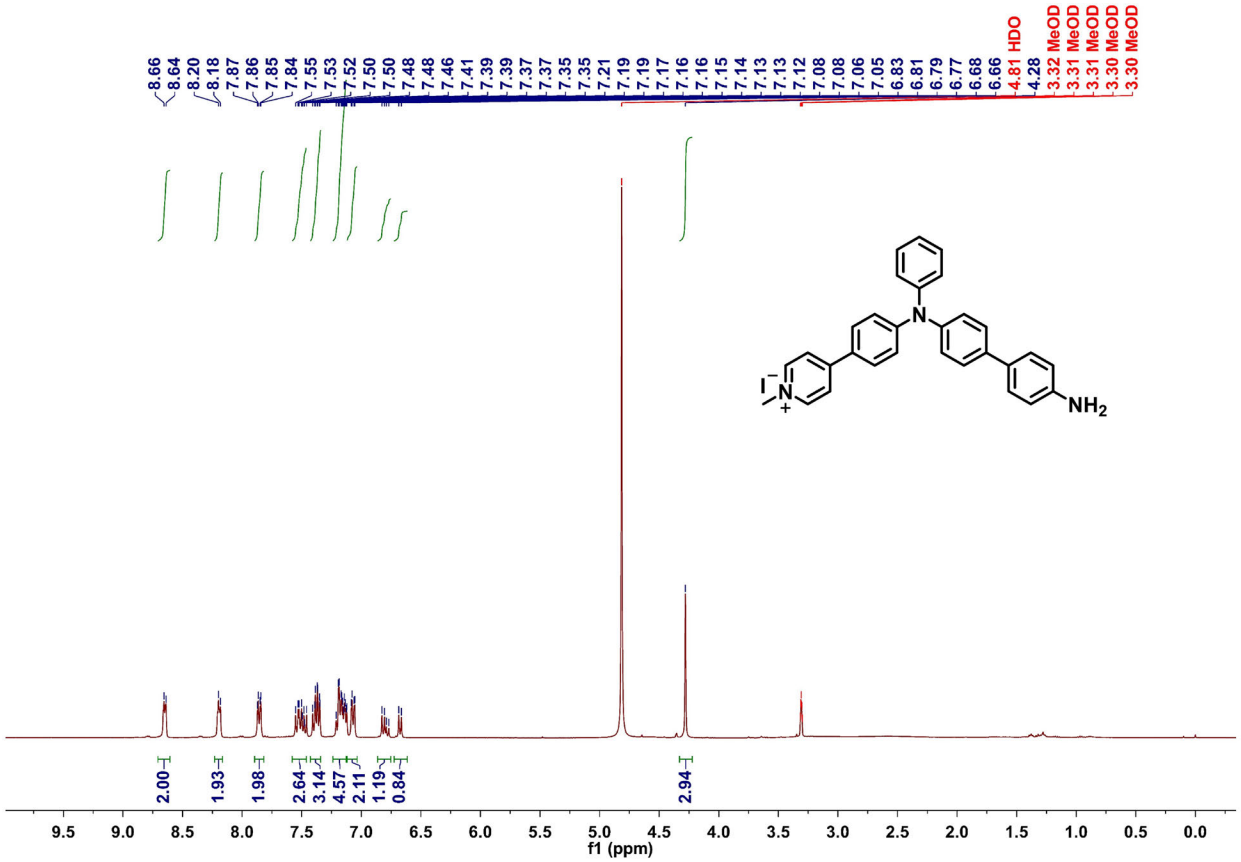

Figure S22. ^{1}H-NMR spectrum of TPA(+) in CD_3OD.

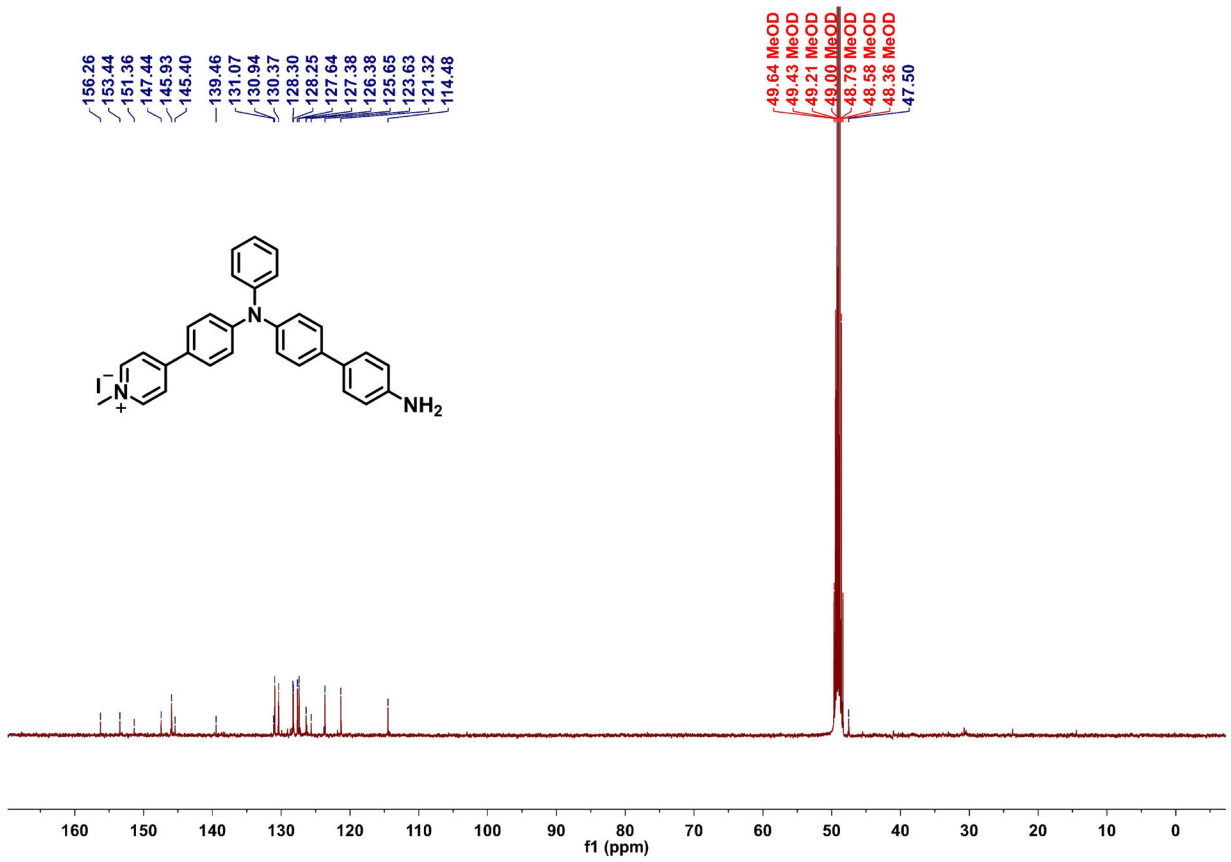

Figure S23. ^{13}C-NMR spectrum of TPA(+) in CD_3OD.

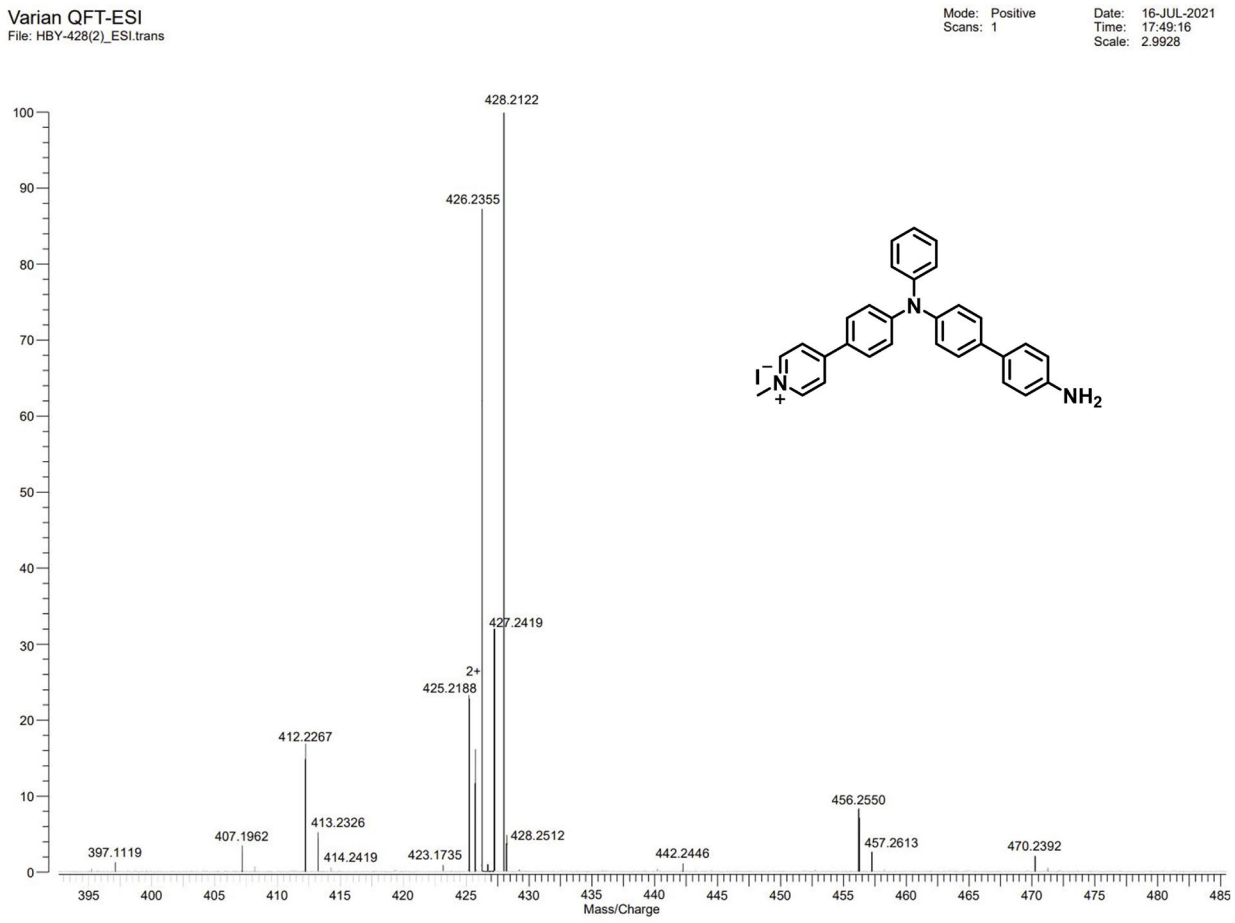

Figure S24. HRMS spectrum of TPA(+).

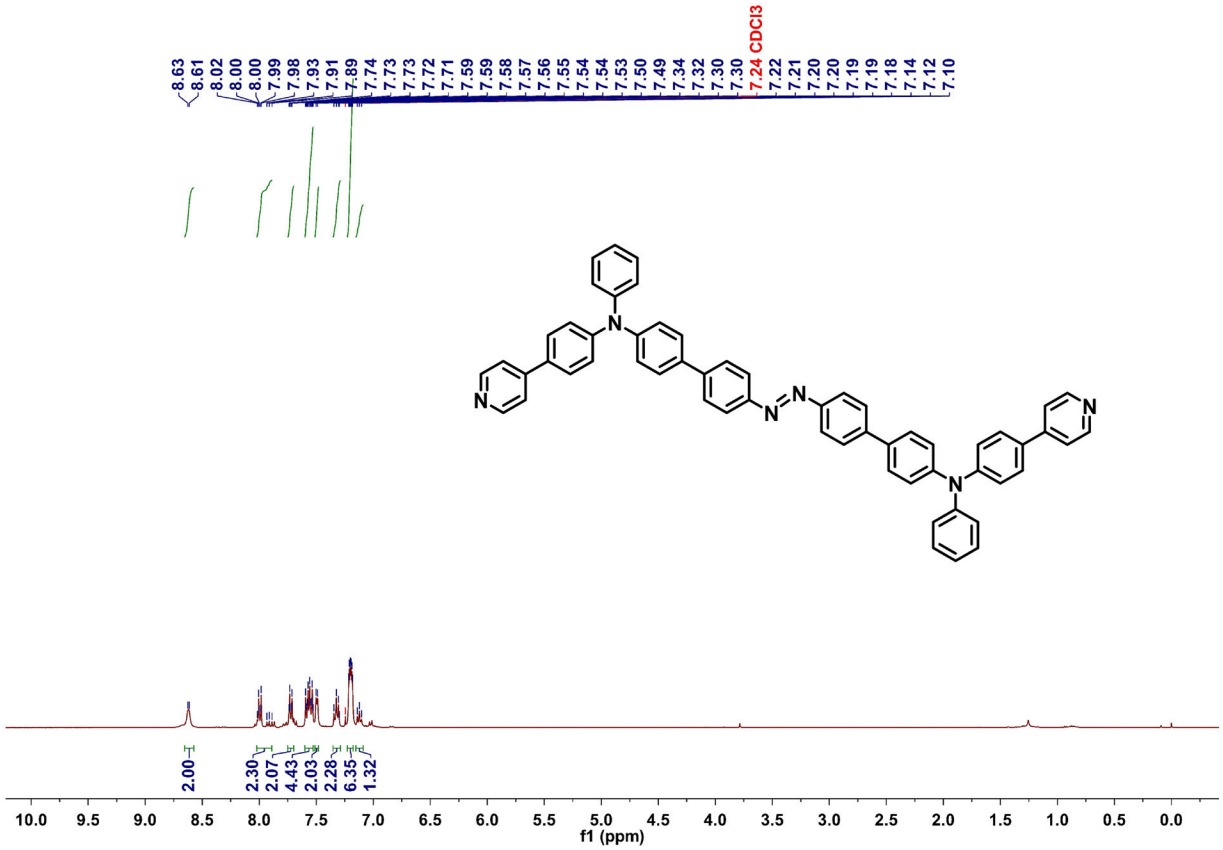

Figure S25. ^{1}H-NMR spectrum of compound **9** in $CDCl_3$.

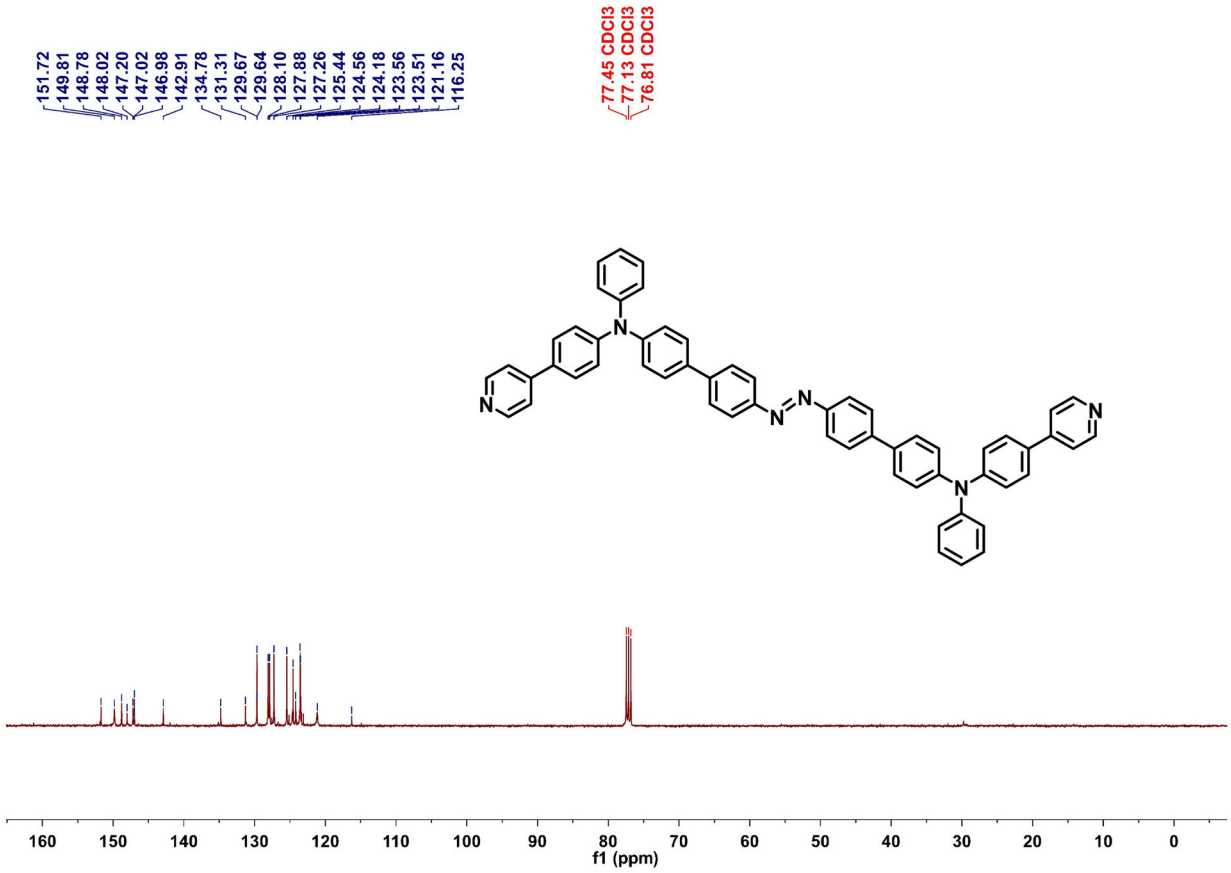

Figure S26. ^{13}C-NMR spectrum of compound **9** in $CDCl_3$.

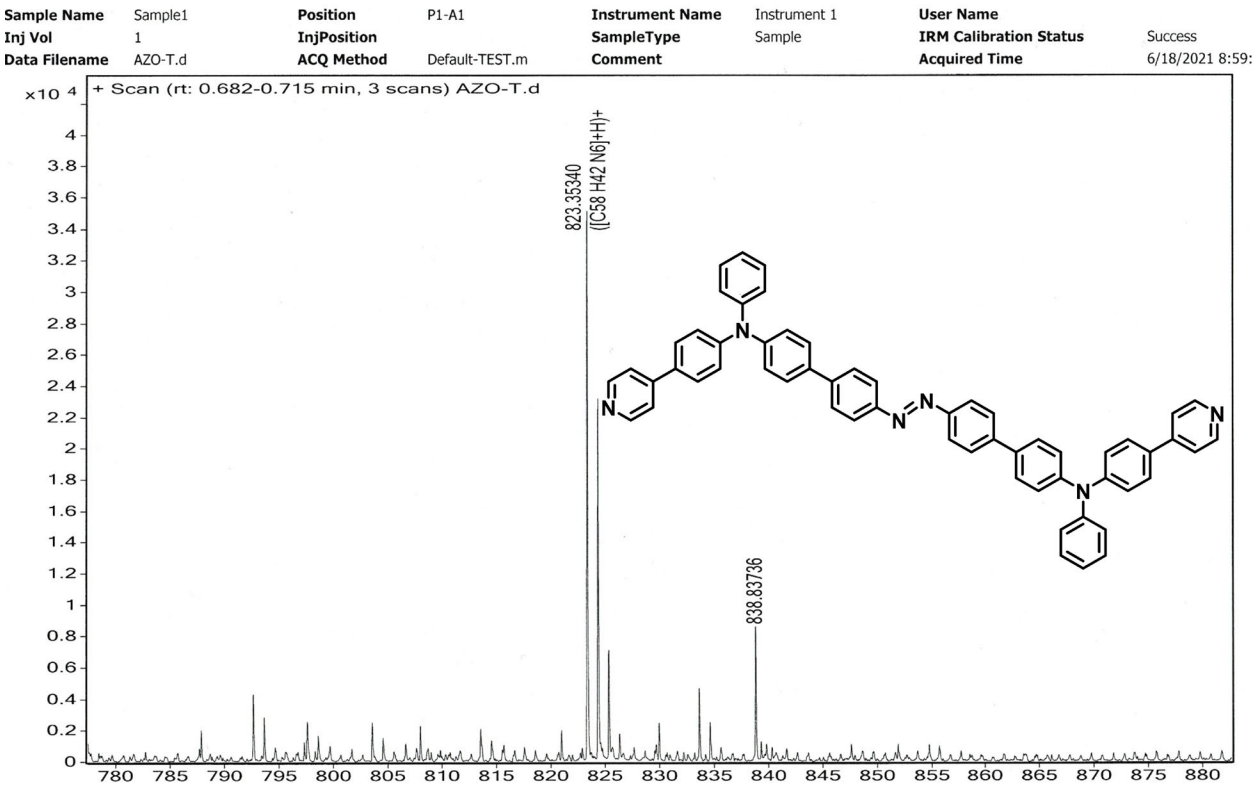

Figure S27. HRMS spectrum of compound **9**.

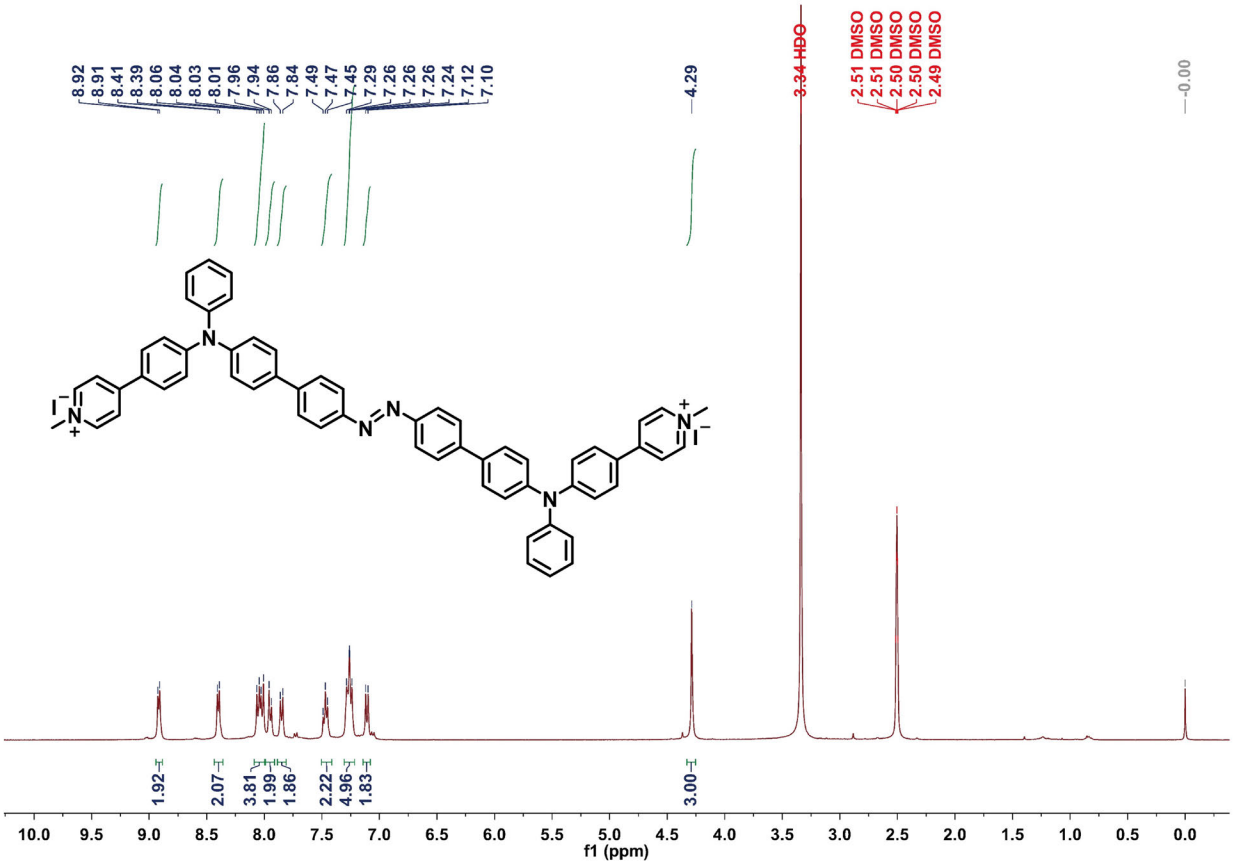

Figure S28. ^{1}H-NMR spectrum of Azo-TPA(+) in DMSO-d_6.

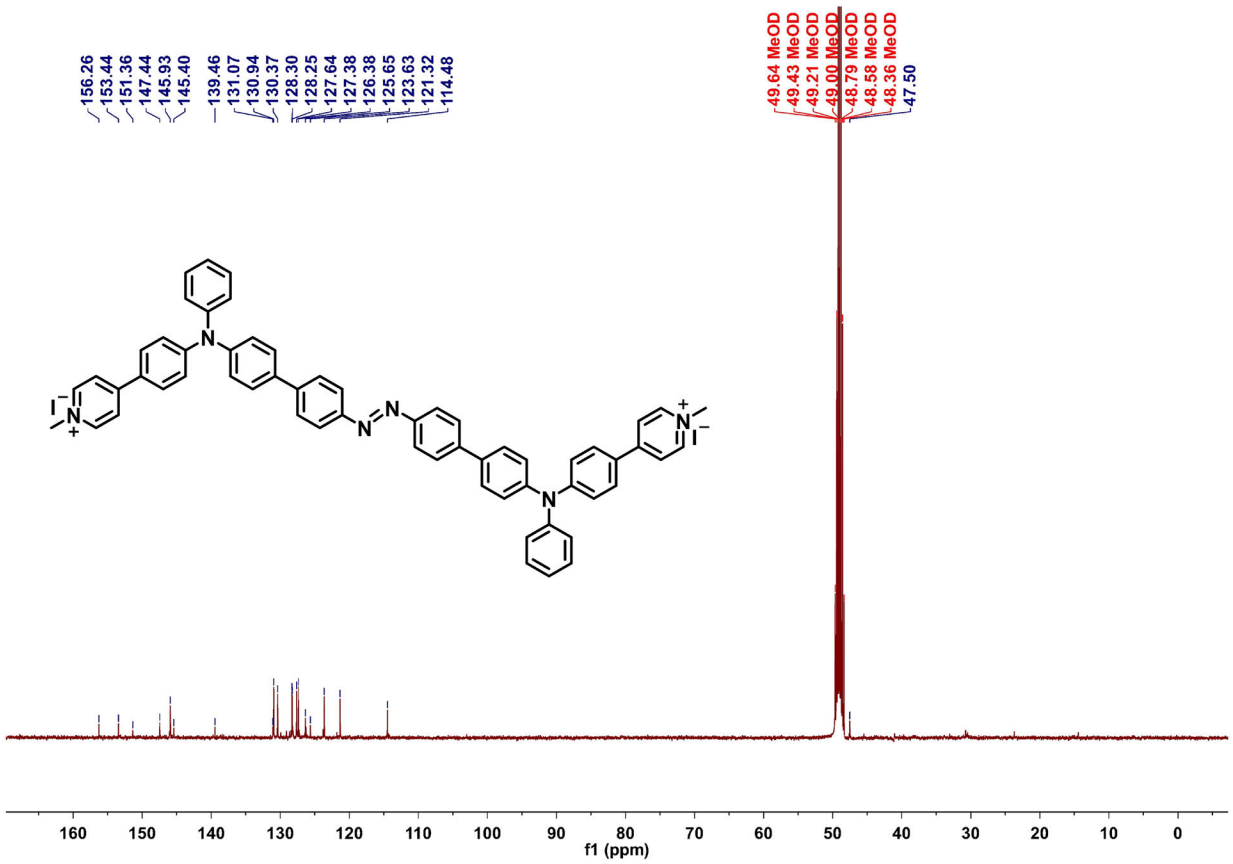

Figure S29. ^{13}C-NMR spectrum of Azo-TPA(+) in DMSO-d_6.

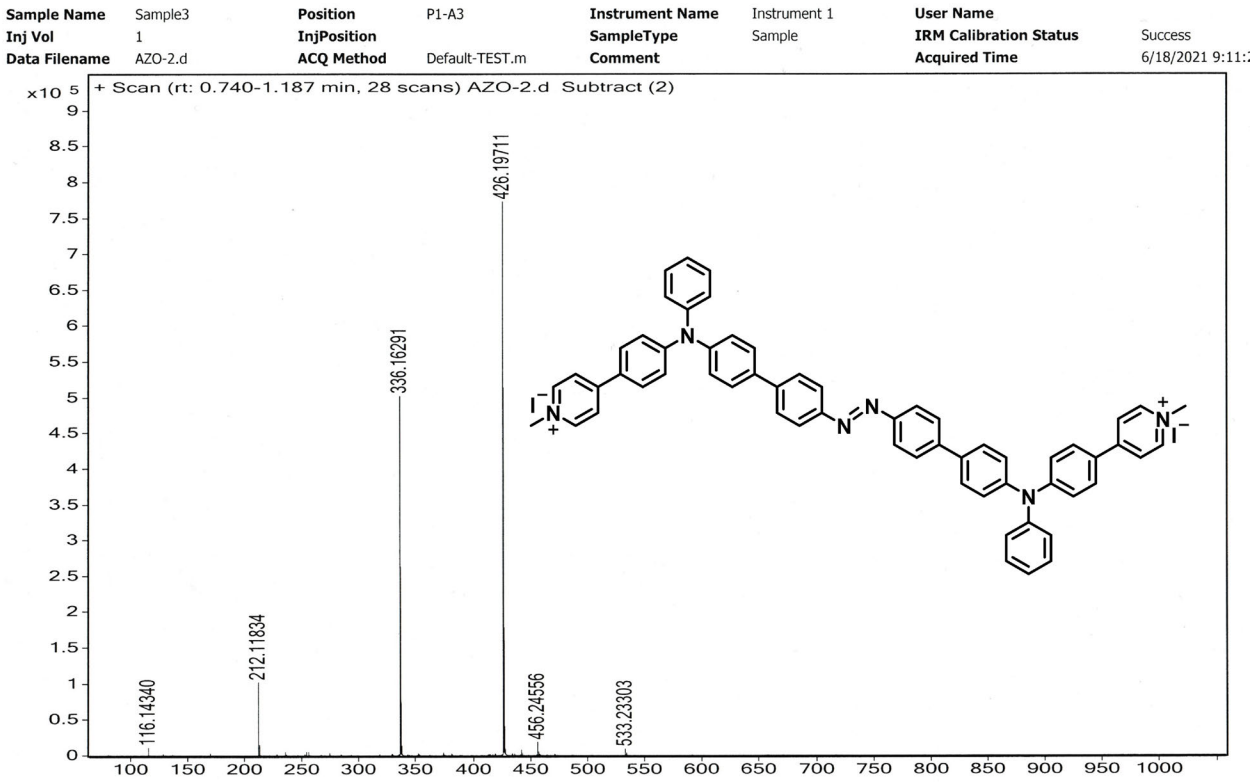

Figure S30. HRMS spectrum of Azo-TPA(+).

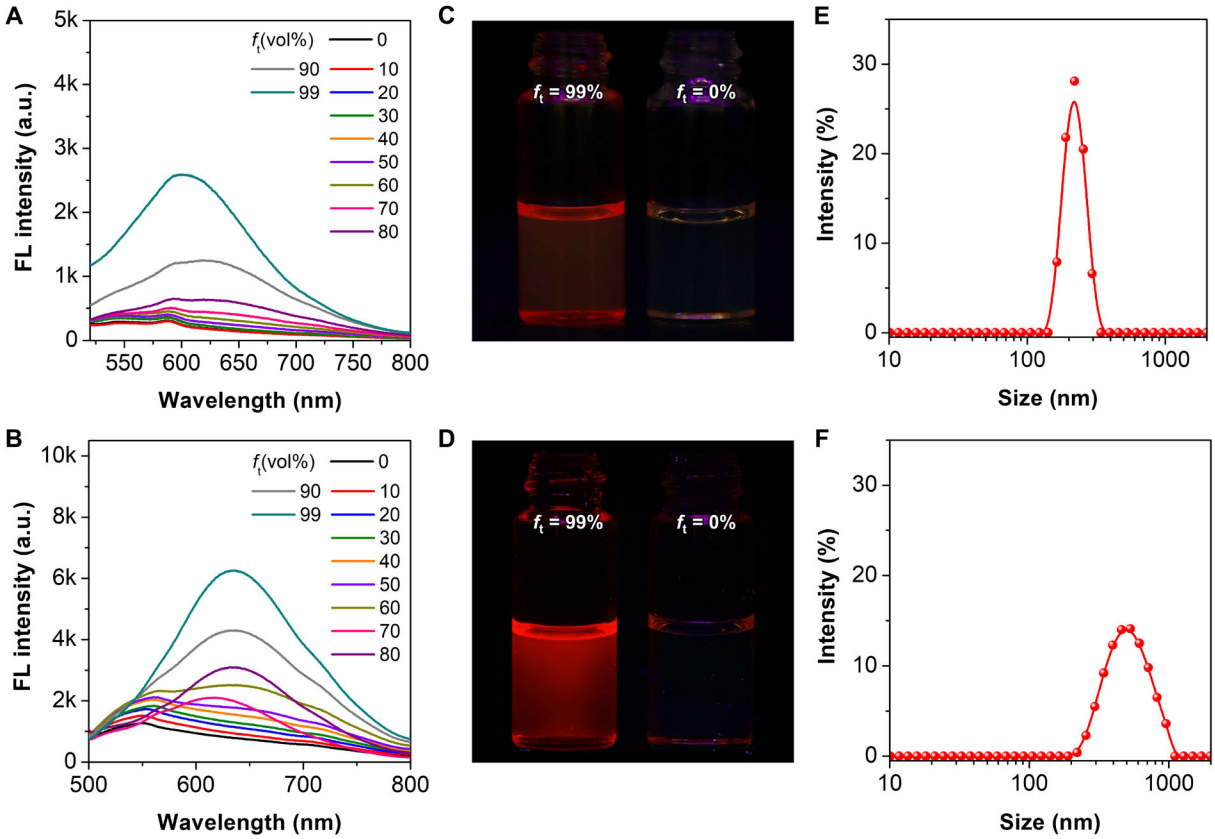

Figure S31. Characterization of AIE properties. Emission spectra of (A) TPA-Th(+) and (B) Azo-TPA-Th(+) in the mixture of DMSO/toluene. Photographs of the solutions of (C) TPA-Th(+) and (D) Azo-TPA-Th(+) at f_t = 0% and f_t = 99% taken under a 365 nm UV lamp. DLS data of the solutions of (E) TPA-Th(+) and (F) Azo-TPA-Th(+) at f_t = 99%.

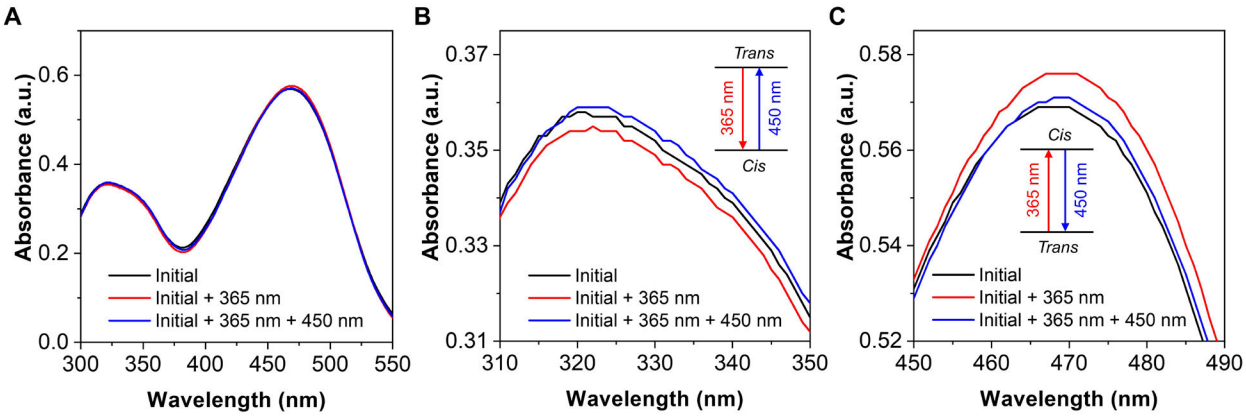

Figure S32. Spectral changes upon light irradiation for Azo-TPA-Th(+) in DMSO (20 μM). (A) UV-vis spectra of Azo-TPA-Th(+) post light irradiation with different wavelength. (B) Enlarged panel (A) with the wavelength ranging from 310 to 350 nm. (C) Enlarged panel (A) with the wavelength ranging from 450 to 490 nm. The sample was exposed to a 365 nm UV light at a power density of 20 mW/cm^2 for 1 min, followed by irradiation with a 450 nm light at a power density of 50 mW/cm^2 for 2 min.

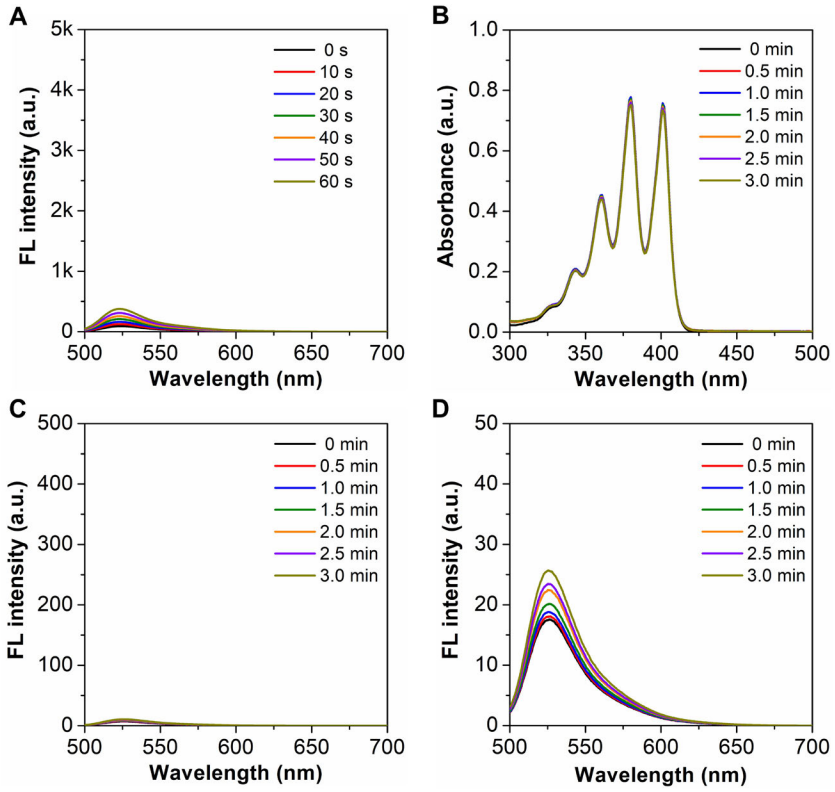

Figure S33. ROS measurements under white light irradiation for the blank group. (A) Emission spectra of DCFH. (B) Absorption spectra of ABDA. (C) Emission spectra of DHR-123. (D) Emission spectra of DHR-123 supplemented with Vc.

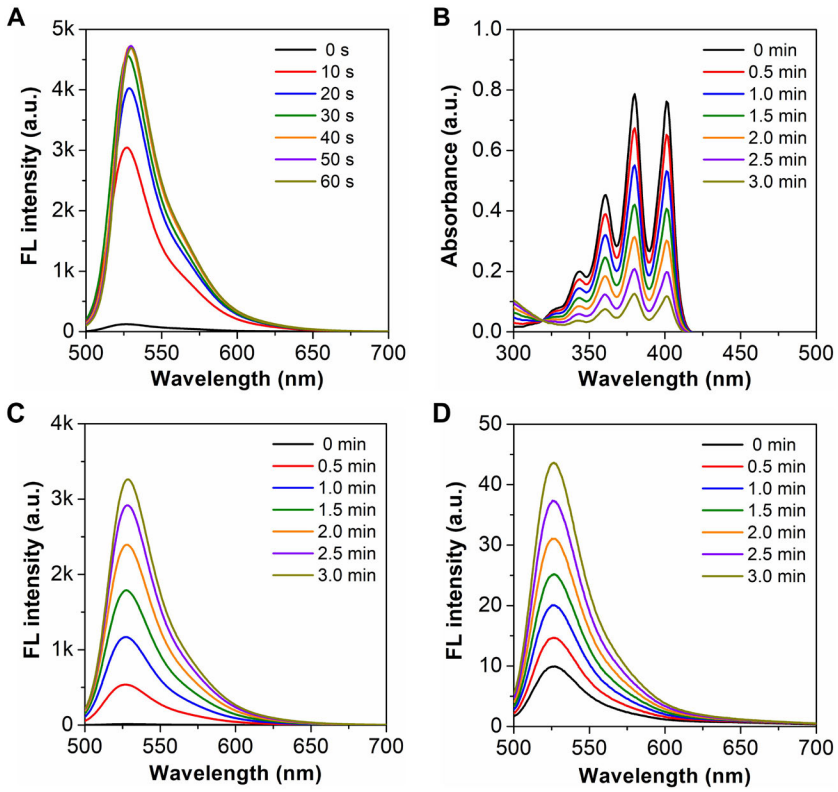

Figure S34. ROS measurements under white light irradiation for the Azo-TPA-Th(+) group. (A) Emission spectra of DCFH in the presence of Azo-TPA-Th(+). (B) Absorption spectra of ABDA in the presence of Azo-TPA-Th(+). (C) Emission spectra of DHR-123 in the presence of Azo-TPA-Th(+). (D) Emission spectra of DHR-123 supplemented with Vc in the presence of Azo-TPA-Th(+).

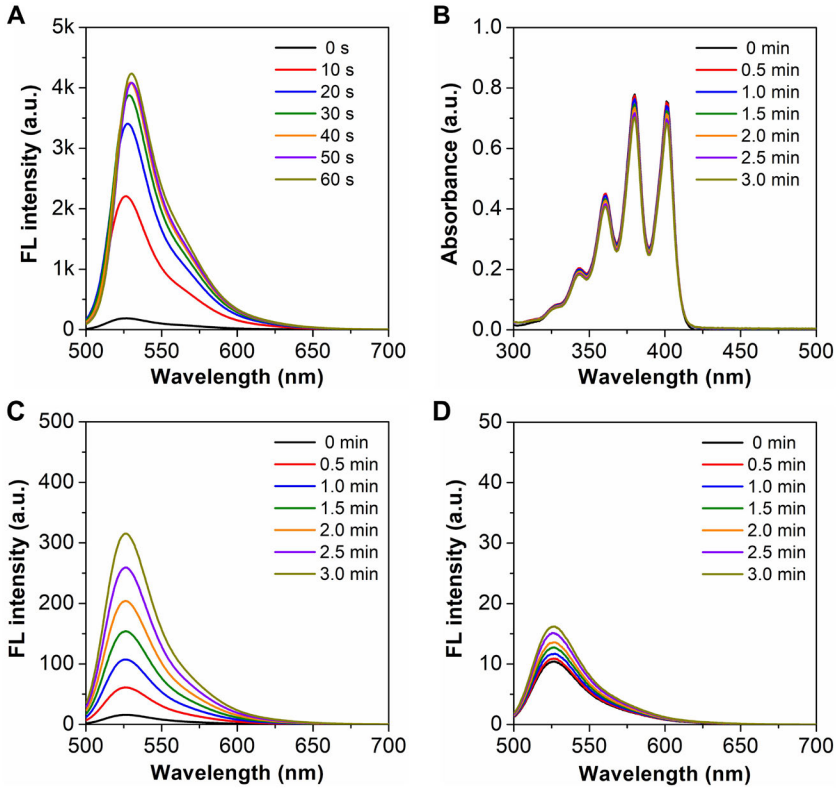

Figure S35. ROS measurements under white light irradiation for the TPA-Th(+) group. (A) Emission spectra of DCFH in the presence of TPA-Th(+). (B) Absorption spectra of ABDA in the presence of TPA-Th(+). (C) Emission spectra of DHR-123 in the presence of TPA-Th(+). (D) Emission spectra of DHR-123 supplemented with Vc in the presence of TPA-Th(+).

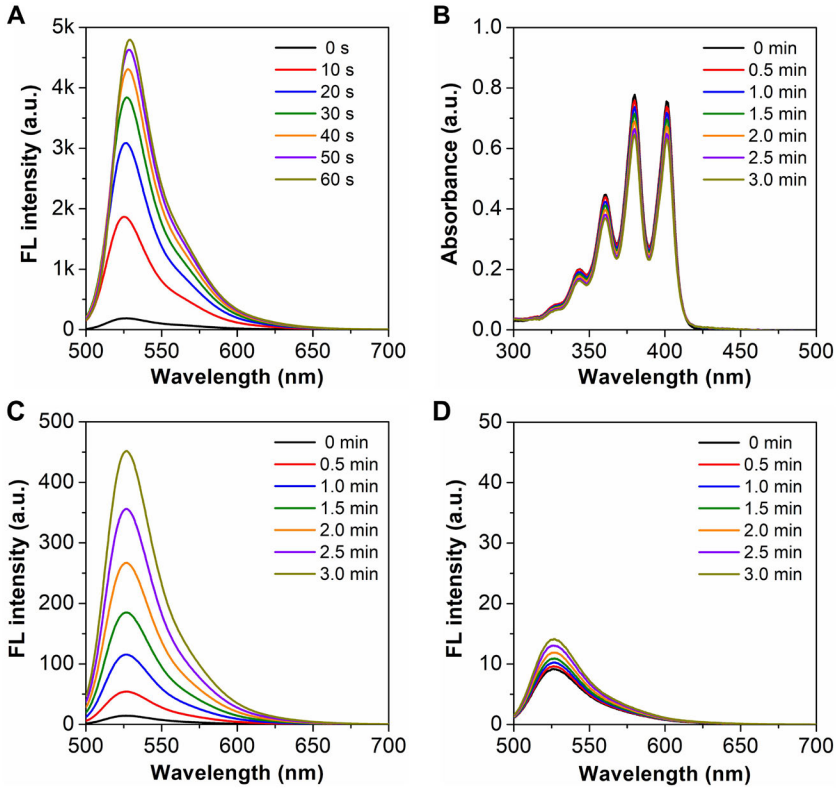

Figure S36. ROS measurements under white light irradiation for the 2 eq TPA-Th(+) group. (A) Emission spectra of DCFH in the presence of 2 eq TPA-Th(+). (B) Absorption spectra of ABDA in the presence of 2 eq TPA-Th(+). (C) Emission spectra of DHR-123 in the presence of 2 eq TPA-Th(+). (D) Emission spectra of DHR-123 supplemented with Vc in the presence of 2 eq TPA-Th(+).

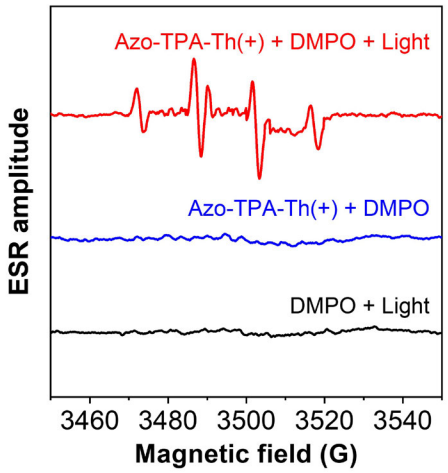

Figure S37. ESR signals of DMPO in the presence of Azo-TPA-Th(+) before and after white light irradiation for $O_2^{\bullet-}$ characterization.

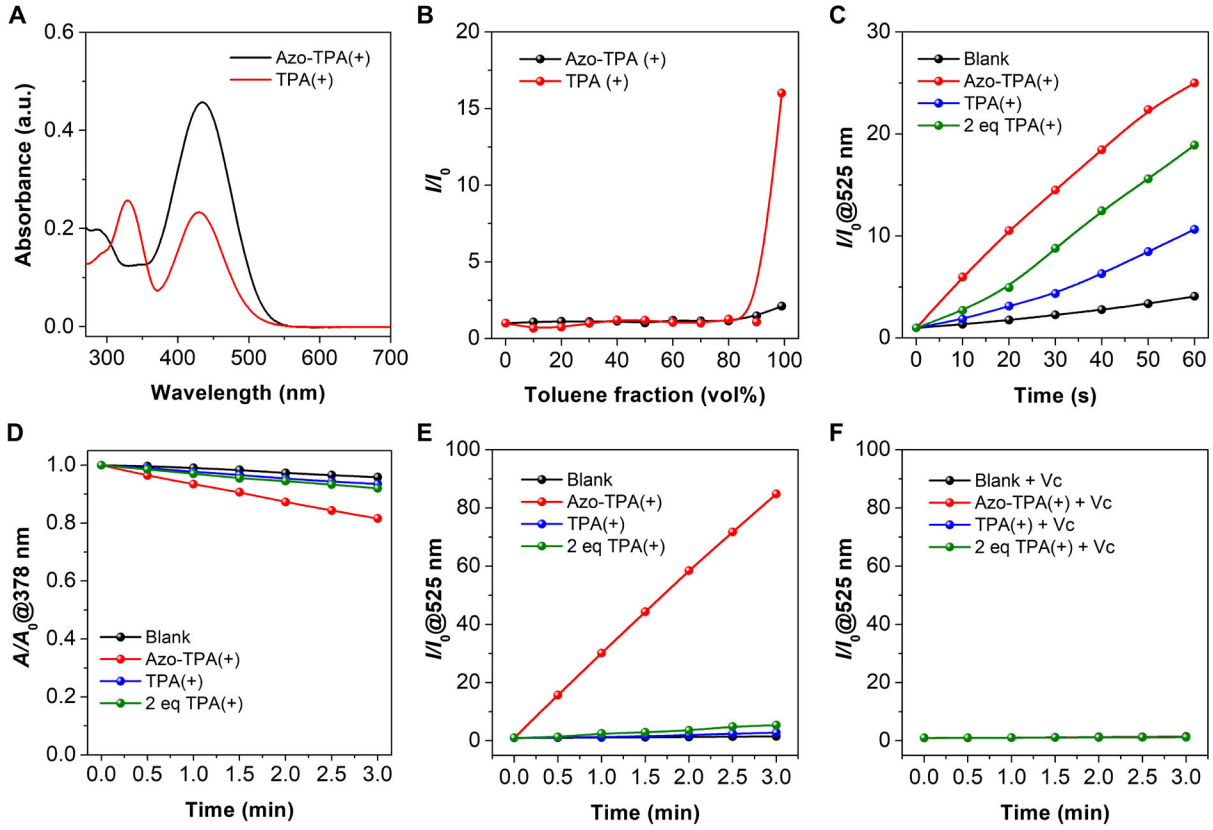

Figure S38. Photophysical and photochemical characterizations of TPA(+) and Azo-TPA(+). (A) UV-vis spectra of Azo-TPA(+) and TPA(+) in DMSO. [Azo-TPA(+)] = [TPA(+)] = 20 μM. (B) Plots of the relative emission intensity (I/I_0) of Azo-TPA(+) at 600 nm and TPA(+) at 515 nm as a function of toluene fractions (f_t) in DMSO/toluene mixtures (Ex = 440 nm). [Azo-TPA(+)] = [TPA(+)] = 20 μM. (C) Plots of the relative emission intensity (I/I_0) at 525 nm of DCFH in the presence of Azo-TPA(+) and TPA(+) upon white light irradiation. (D) Decomposition rate of ABDA in the presence of Azo-TPA(+) and TPA(+) upon white light irradiation. A_0 and A represent the absorbance at 378 nm before and after white light irradiation, respectively. (E) Plots of the relative emission intensity (I/I_0) at 525 nm of DHR-123 in the presence of Azo-TPA(+) and TPA(+) as a function of irradiation time. (F) Plots of the relative emission intensity (I/I_0) at 525 nm of DHR-123 in the presence of Azo-TPA(+) and TPA(+) supplemented with Vc as a function of irradiation time.

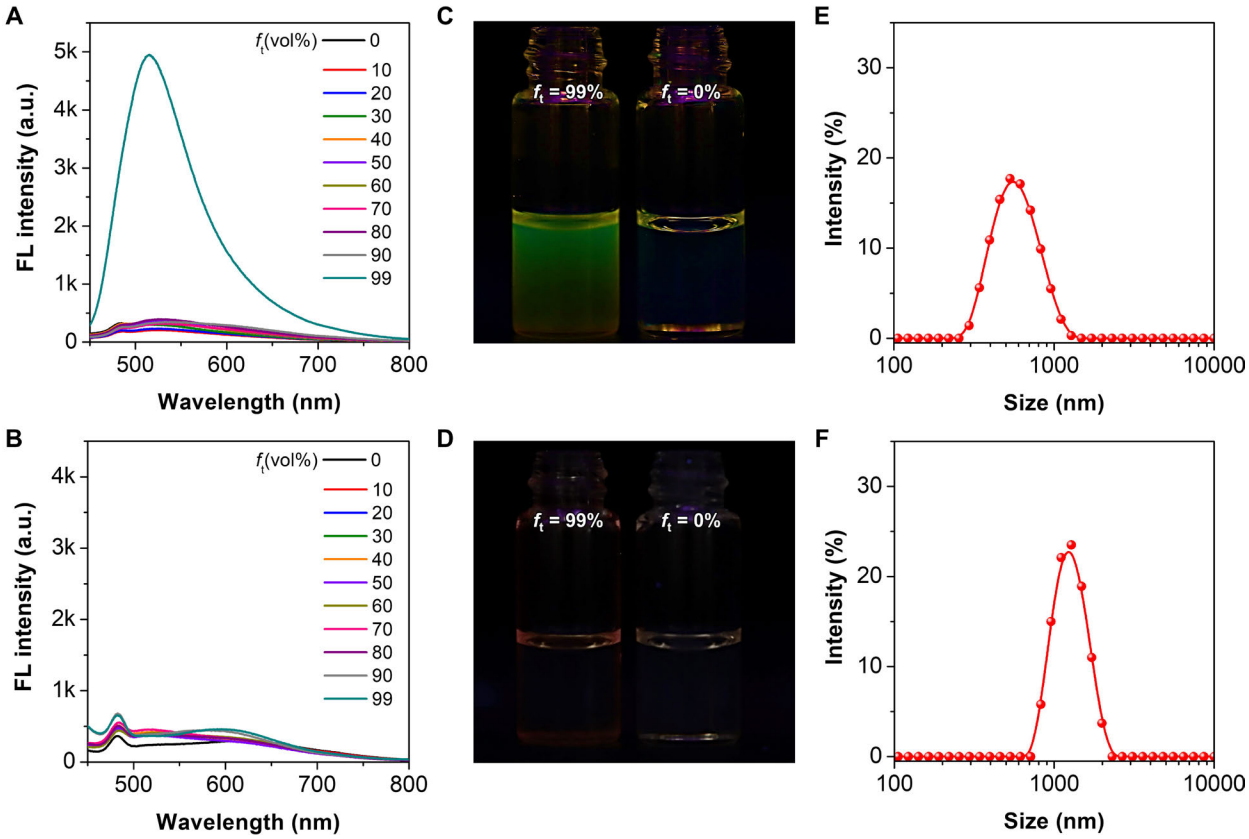

Figure S39. Characterization of AIE properties. Emission spectra of (A) TPA(+) and (B) Azo-TPA(+) in the mixture of DMSO/toluene. Photographs of the solutions of (C) TPA(+) and (D) Azo-TPA(+) at f_t = 0% and f_t = 99% taken under a 365 nm UV lamp. DLS data of the solutions of (E) TPA(+) and (F) Azo-TPA(+) at f_t = 99%.

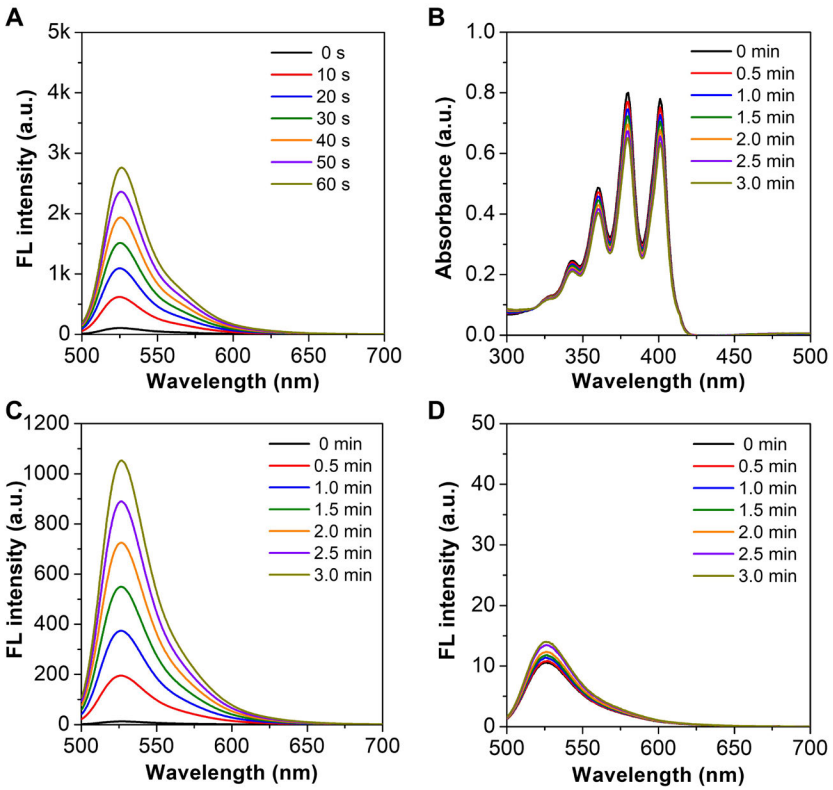

Figure S40. ROS measurements under white light irradiation for the Azo-TPA(+) group. (A) Emission spectra of DCFH in the presence of Azo-TPA(+). (B) Absorption spectra of ABDA in the presence of Azo-TPA(+). (C) Emission spectra of DHR-123 in the presence of Azo-TPA(+). (D) Emission spectra of DHR-123 supplemented with Vc in the presence of Azo-TPA(+).

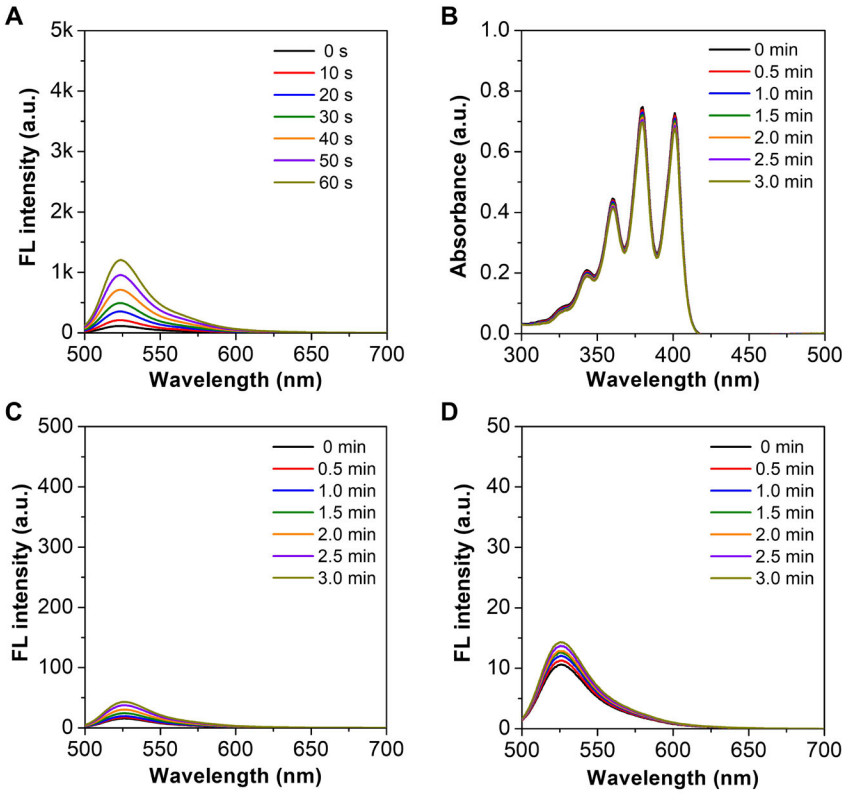

Figure S41. ROS measurements under white light irradiation for the TPA(+) group. (A) Emission spectra of DCFH in the presence of TPA(+). (B) Absorption spectra of ABDA in the presence of TPA(+). (C) Emission spectra of DHR-123 in the presence of TPA(+). (D) Emission spectra of DHR-123 supplemented with Vc in the presence of TPA(+).

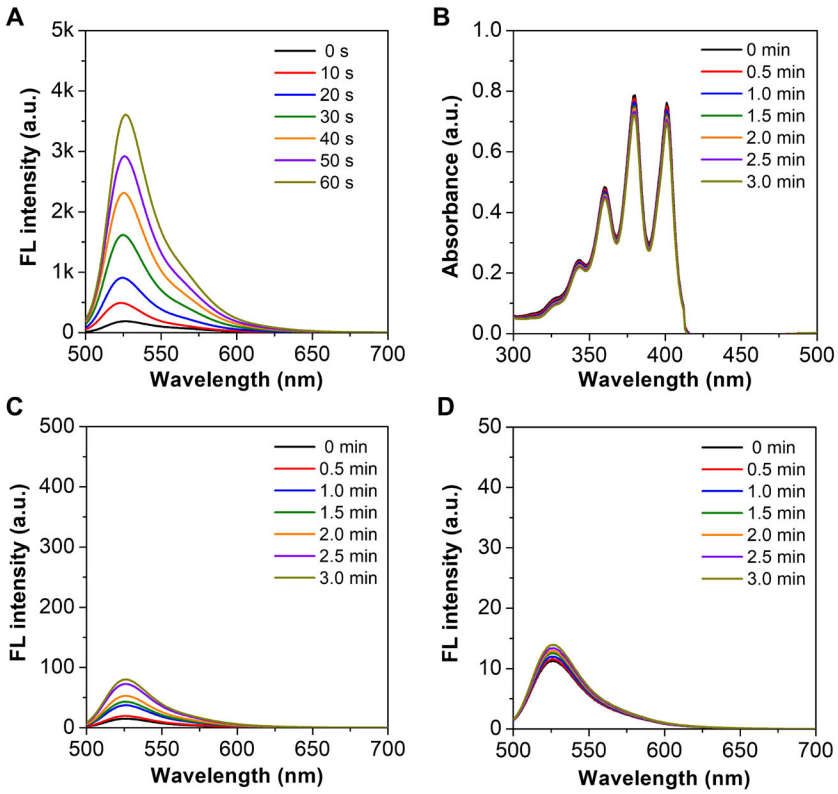

Figure S42. ROS measurements under white light irradiation for the 2 eq TPA(+) group. (A) Emission spectra of DCFH in the presence of 2 eq TPA(+). (B) Absorption spectra of ABDA in the presence of 2 eq TPA(+). (C) Emission spectra of DHR-123 in the presence of 2 eq TPA(+). (D) Emission spectra of DHR-123 supplemented with Vc in the presence of 2 eq TPA(+).

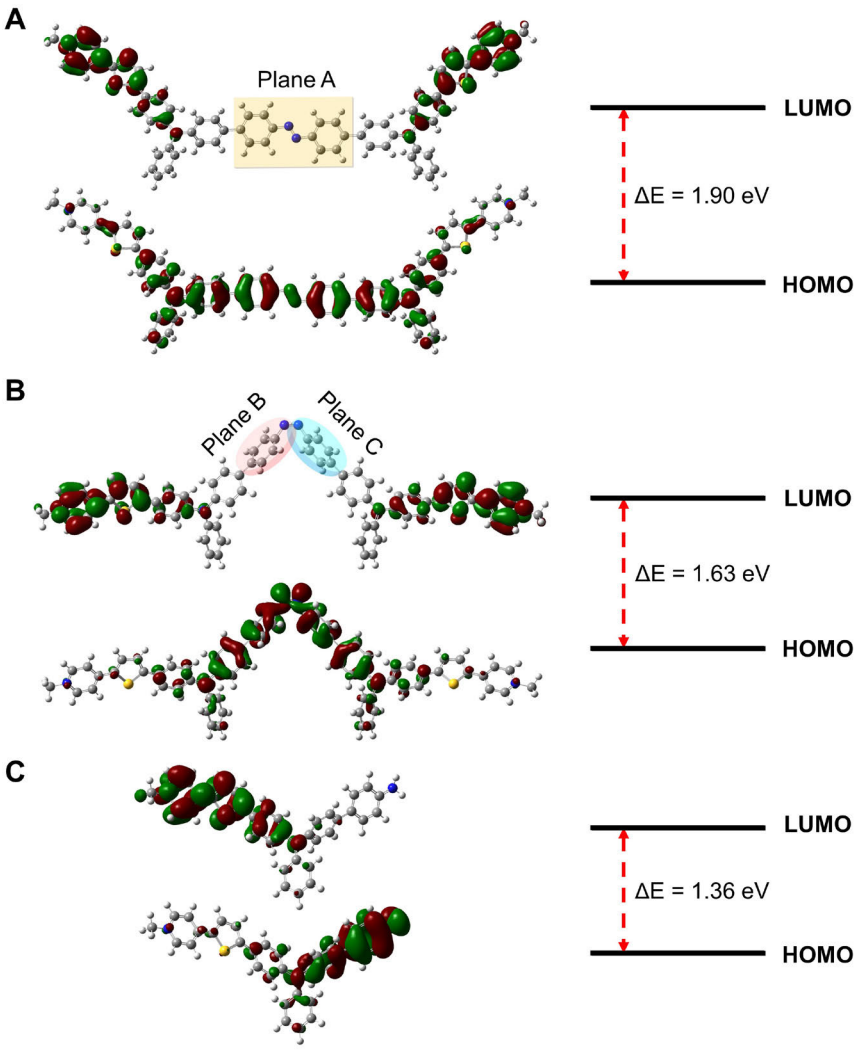

Figure S43. Calculated FMOs and corresponding energies of (A) *trans*-Azo-TPA-Th(+), (B) *cis*-Azo-TPA-Th(+), and (C) TPA-Th(+).

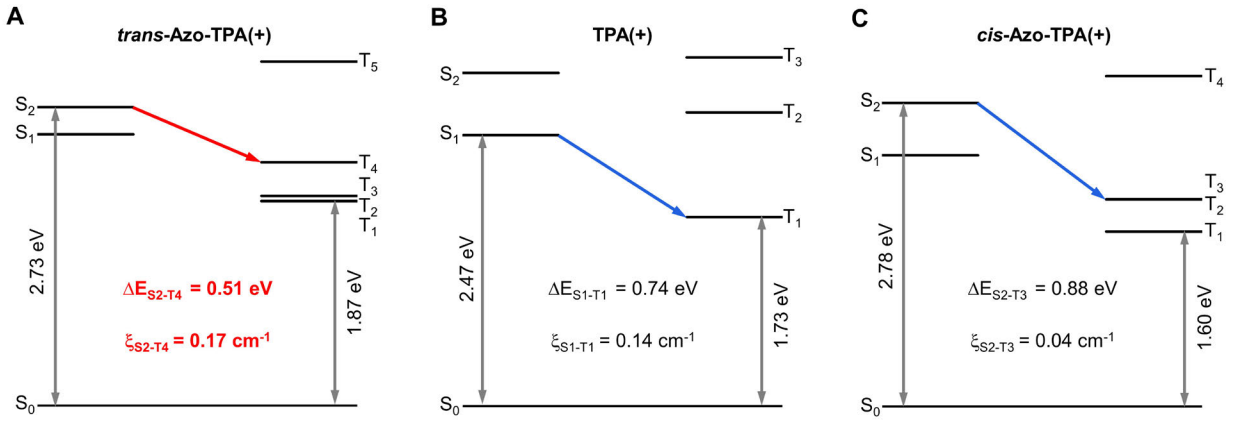

Figure S44. Energy level diagrams and calculated ξ_{ST} between different singlet-triplet channels for (A) *trans*-Azo-TPA(+), (B) TPA(+), and (C) *cis*-Azo-TPA(+).

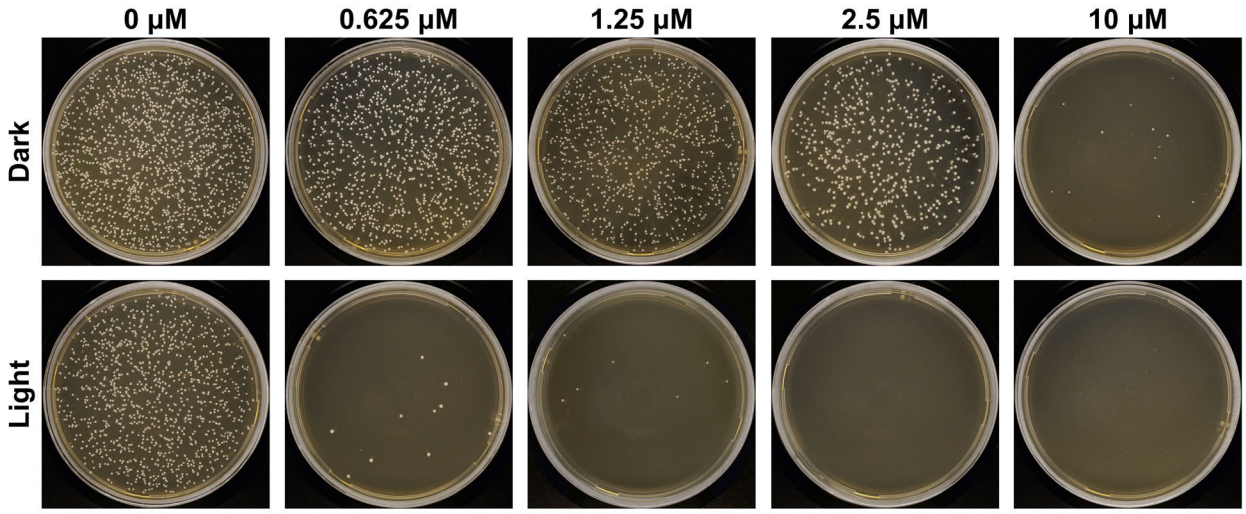

Figure S45. Photographs of bacterial colonies formed on agar plates after incubation with varying concentrations of Azo-TPA-Th(+) in the absence and presence of white light irradiation.

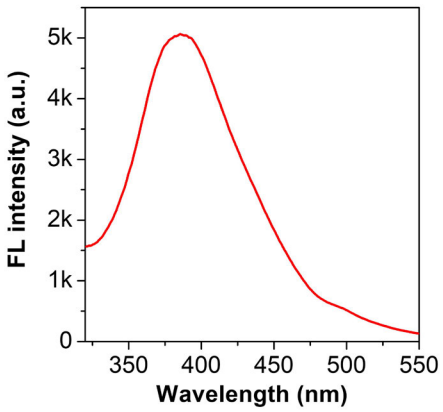

Figure S46. Excitation spectrum of Azo-TPA-Th(+) in PBS (Em = 460 nm).

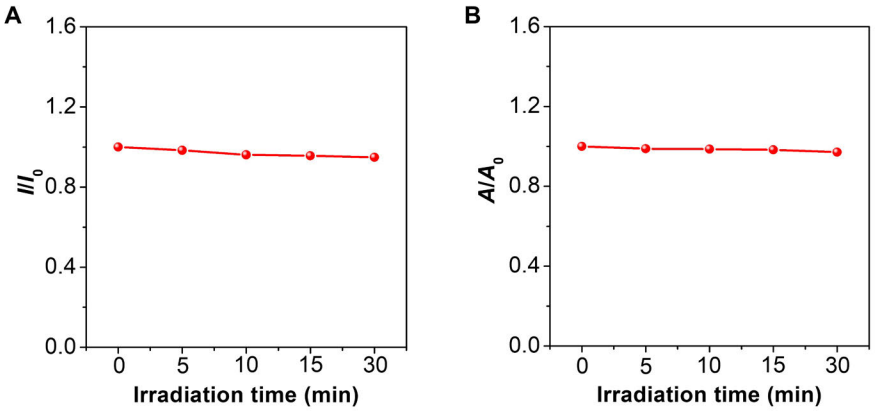

Figure S47. Irradiation of Azo-TPA-Th(+) in DMSO with a 365 nm UV light. (A) Plot of the relative absorbance (A/A_0) at the absorption maximum. A_0 represents the absorbance before UV irradiation, and A represents the absorbance at different time points post UV irradiation. (B) Plot of the relative emission intensity at 460 nm. I_0 represents the emission intensity before UV irradiation, and I represents the emission intensity at different time points post UV irradiation.

Table S1. Theoretically calculated energy levels, oscillator strength, energy gaps, and SOC constants of *trans*-Azo-TPA-Th(+).

S_n	*f*	E_{Sn} (eV)	T_n	E_{Tn} (eV)	S_2-T_n	$\Delta E_{S2\text{-}Tn}$ (eV)	$\xi_{S2\text{-}Tn}$ (cm^{-1})	S_1-T_n	$\Delta E_{S1\text{-}Tn}$ (eV)	$\xi_{S1\text{-}Tn}$ (cm^{-1})
S_1	1.94	2.19	T_1	1.38	S_2-T_1	0.85	0.04	S_1-T_1	0.81	0.02
S_2	1.12	2.23	T_2	1.38	S_2-T_2	0.85	0.05	S_1-T_2	0.81	0.02
S_3	0	2.49	T_3	1.93	S_2-T_3	0.30	0.20	S_1-T_3	0.26	0
S_4	0.03	2.95	T_4	2.22	S_2-T_4	0.01	0.28	S_1-T_4	-0.03	0.04
S_5	0.10	2.96	T_5	2.60	S_2-T_5	-0.37	0.52	S_1-T_5	-0.41	0.20

Table S2. Theoretically calculated energy levels, oscillator strength, energy gaps, and SOC constants of TPA-Th(+).

S_n	f	E_{Sn} (eV)	T_n	E_{Tn} (eV)	S_1-T_n	$\Delta E_{S1\text{-}Tn}$ (eV)	$\xi_{S1\text{-}Tn}$ (cm^{-1})
S_1	1.11	2.05	T_1	1.26	S_1-T_1	0.79	0.32
S_2	0.38	2.59	T_2	2.31	S_1-T_2	-0.26	0.23
S_3	0.20	3.54	T_3	2.75	S_1-T_3	-0.70	0.79
S_4	0.04	3.55	T_4	3.11	S_1-T_4	-1.06	0.33
S_5	0.11	3.88	T_5	3.22	S_1-T_5	-1.17	0.35

Table S3. Theoretically calculated energy levels, oscillator strength, energy gaps, and SOC constants of *cis*-Azo-TPA-Th(+).

S_n	*f*	E_{Sn} (eV)	T_n	E_{Tn} (eV)	S_1-T_n	$\Delta E_{S1\text{-}Tn}$ (eV)	$\xi_{S1\text{-}Tn}$ (cm^{-1})
S_1	2.83	2.21	T_1	1.41	S_1-T_1	0.80	0.02
S_2	0	2.26	T_2	1.41	S_1-T_2	0.80	0.06
S_3	0.08	2.34	T_3	1.63	S_1-T_3	0.58	0.08
S_4	0	2.93	T_4	2.61	S_1-T_4	-0.40	0.42
S_5	0.07	2.93	T_5	2.61	S_1-T_5	-0.40	0.44

Table S4. Theoretically calculated energy levels, oscillator strength, energy gaps, and SOC constants of *trans*-Azo-TPA(+).

S_n	f	E_{Sn} (eV)	T_n	E_{Tn} (eV)	S_2-T_n	$\Delta E_{S2\text{-}Tn}$ (eV)	$\xi_{S2\text{-}Tn}$ (cm^{-1})
S_1	0	2.48	T_1	1.87	S_2-T_1	0.86	0.02
S_2	2.50	2.73	T_2	1.87	S_2-T_2	0.86	0.06
S_3	0.10	2.78	T_3	1.92	S_2-T_3	0.81	0.01
S_4	0.81	3.48	T_4	2.22	S_2-T_4	0.51	0.17
S_5	0.01	3.51	T_5	3.15	S_2-T_5	-0.42	0.03

Table S5. Theoretically calculated energy levels, oscillator strength, energy gaps, and SOC constants of TPA(+).

S_n	f	E_{Sn} (eV)	T_n	E_{Tn} (eV)	S_1-T_n	$\Delta E_{S1\text{-}Tn}$ (eV)	$\xi_{S1\text{-}Tn}$ (cm^{-1})
S_1	0.63	2.47	T_1	1.73	S_1-T_1	0.74	0.14
S_2	0.59	3.05	T_2	2.69	S_1-T_2	-0.22	0.32
S_3	0	3.64	T_3	3.19	S_1-T_3	-0.72	0.35
S_4	0.14	4.21	T_4	3.34	S_1-T_4	-0.87	0.05
S_5	0.27	4.26	T_5	3.65	S_1-T_5	-1.18	0.28

Table S6. Theoretically calculated energy levels, oscillator strength, energy gaps, and SOC constants of *cis*-Azo-TPA(+).

S_n	f	E_{Sn} (eV)	T_n	E_{Tn} (eV)	S_2-T_n	$\Delta E_{S2\text{-}Tn}$ (eV)	$\xi_{S2\text{-}Tn}$ (cm^{-1})
S_1	0.05	2.30	T_1	1.60	S_2-T_1	1.18	0.06
S_2	2.26	2.78	T_2	1.90	S_2-T_2	0.88	0.04
S_3	0.02	2.81	T_3	1.90	S_2-T_3	0.88	0.04
S_4	0.02	3.42	T_4	3.03	S_2-T_4	-0.25	0.12
S_5	0.13	3.42	T_5	3.10	S_2-T_5	-0.32	0.47

Table S7. VIPs and VEAs of all PSs with water as the solvent.

Compound	VIP_{S0} (eV)	VIP_{T1} (eV)	VEA_{S0} (eV)	VEA_{T1} (eV)	$VIP_{T1} + AEA_{O2}$ (eV)
trans-Azo-TPA-Th(+)	5.23	3.30	-3.15	-5.07	-0.61
TPA-Th(+)	5.09	3.47	-3.17	-4.80	-0.44
cis-Azo-TPA-Th(+)	5.22	3.51	-3.13	-4.84	-0.40
trans-Azo-TPA (+)	5.43	3.42	-3.08	-5.08	-0.49
TPA (+)	5.26	3.29	-2.90	-4.88	-0.62
cis-Azo-TPA (+)	5.42	3.69	-2.91	-4.64	-0.22

Note: As depicted in the equation of $PS(T_1) + {}^3O_2 \rightarrow PS(T_1)^{\bullet+} + O_2^{\bullet-}$, T_1 state PSs can sensitize the generation of $O_2^{\bullet-}$ by donating an electron to oxygen. The prerequisite for this reaction is that the summation of the VIP for the T_1 state (VIP_{T1}) of PSs and the adiabatic electron affinity (AEA) of ${}^3O_2$ (AEA_{O2}; -3.91 eV in water) should be negative.